PERIPHERAL NEUROPATHIES

New technologies for the assessment of neuropathies

Roberto Gasparotti[1], Luca Padua[2,3], Chiara Briani[4] and Giuseppe Lauria[5]

Abstract | Technical advances are rapidly changing the clinical and instrumental approach to peripheral nerve diseases. Magnetic resonance neurography, diffusion tensor imaging and nerve ultrasonography are increasingly entering the diagnostic workup of peripheral neuropathies as tools that complement neurophysiology and enable investigation of proximal structures, such as plexuses and roots. Progress in the design of magnetic resonance scanners and sequences, and the development of high-frequency ultrasound probes mean that high-resolution peripheral nerve imaging is possible, enabling detailed examination of nerve size, morphology and internal fascicular structure that can integrate nerve conduction studies into clinical practice. In the growing field of small-fibre neuropathy, in which traditional nerve conduction studies are of little or no use, skin biopsy has become a reliable tool for diagnosis. Corneal confocal microscopy, nociceptive evoked potentials and microneurography are emerging techniques that are mainly used in clinical research settings, but have increasing relevance to clinical practice. We review these new and emerging techniques and their effects on diagnosis, treatment strategies and prognosis in a variety of peripheral neuropathies, including entrapments, brachial plexopathies, immune and inherited neuropathies, and small-fibre neuropathies. We discuss the most promising research findings and their potential for future application in clinical practice.

[1]*Department of Medical and Surgical Specialties, Radiological Sciences, and Public Health, University of Brescia, Neuroradiology Unit, Spedali Civili, Piazza Spedali Civili 1–25123 Brescia, Italy.*
[2]*Catholic University, Department of Geriatrics, Neurology, Orthopedics and Rehabilitation, Largo Agostino Gemelli 8, 0630151, Rome, Italy.*
[3]*Fondazione Don Gnocchi, P.le R. Morandi 6, 20121 Milan, Italy.*
[4]*Department of Neurosciences, University of Padova, Via Giustiniani 5, 35128 Padova, Italy.*
[5]*Neuroalgology Unit and Skin Biopsy, Peripheral Neuropathy and Neuropathic Pain Laboratory, IRCCS Foundation "Carlo Besta" Neurological Institute, Via Celoria 11, 20133 Milan, Italy.*

Correspondence to R.G.
roberto.gasparotti@unibs.it

doi:10.1038/nrneurol.2017.31
Published online 17 Mar 2017

Peripheral neuropathies are among the most common neurological disorders[1]. In routine clinical practice, diagnosis of peripheral neuropathies is typically based on clinical assessment, nerve conduction studies and needle electromyography, which can determine whether symptoms are caused by primary axonal damage or demyelinating damage. This distinction is often relevant to therapeutic choices and to prognosis, as axonal damage typically reflects an inflammatory (for example, vasculitic) or degenerative (for example, hereditary or idiopathic) process that correlates with disability, whereas demyelinating damage can reflect a hereditary neuropathy, but more often reflects an acquired immune-mediated neuropathy. Besides metabolic, inflammatory or primary degenerative neuropathies, peripheral nerves can also be damaged by compression from adjacent tissue structures, such as tendons, cysts or haematomas. In this case, proper identification of the site, nature and degree of the lesion might be challenging, but is relevant to treatment and prognosis. Moreover, some patients present with symptoms that suggest damage to small nerve fibres, which nerve conduction studies cannot be used to detect.

In the past 15 years, several techniques have become available to investigate focal and diffuse peripheral neuropathies, and their reliability has widened the spectrum of diagnostic tools for clinicians and improved assessment of neuropathies. In this Review, we provide an overview of these new and emerging technologies. We first discuss peripheral nerve imaging with MRI and ultrasonography, which can provide information about the precise localization of neuropathies and the pathological processes involved in large-fibre neuropathies, and can complement clinical and electrophysiological evaluation. We then consider techniques that can provide diagnostic information when the pathological process is restricted to small nerve fibres and is consequently not detectable with nerve conduction studies or neuroimaging. These include skin biopsy, which is established in clinical practice, and the emerging techniques of corneal confocal microscopy, laser-evoked potentials and heat-related and pain-related evoked potentials, and microneurography.

Nerve imaging technology

Advances in imaging techniques have made it possible to gain great insight into nerve pathology with magnetic resonance and ultrasound. Each approach offers distinct advantages, and can provide different information about damage to large myelinated fibres.

Key points

- Ultrasonography has an established role in the investigation of nerve entrapment syndromes and ambiguous neurophysiological findings, and an emerging role in the assessment of diffuse polyneuropathies
- Magnetic resonance neurography has a supportive role in the diagnostic workup of inflammatory neuropathies, can provide additional information in entrapment neuropathies and has an emerging role in diffuse polyneuropathies
- Skin biopsy is a minimally invasive technique for diagnosing small-fibre neuropathies, can be used to assess large myelinated nerve fibres, and can provide a quantitative assessment of autonomic pathology
- Confocal corneal microscopy is a noninvasive technique for detecting small-fibre loss in neuropathies, and findings with this technique correlate with those of skin biopsy in small-fibre neuropathies
- Microneurography is a minimally invasive technique for the investigation of physiological properties and pathological changes in small-nerve fibres

Magnetic resonance neurography

Conventional MRI provides poor visualization of peripheral nerves, owing to the small size of the nerves and their low contrast with surrounding vessels and muscles. The development of magnetic resonance neurography (MRN) has overcome these limitations. This imaging technique is based on T2-weighted sequences in which fat suppression is used, enabling the assessment of specific nerve morphological features, such as calibre, internal fascicular pattern and the amount of perineurial–endoneurial fluid[2].

In the past 15 years, technological advances such as parallel imaging, coil design and new pulse sequences, combined with the clinical availability of 3T magnetic resonance scanners, have led to the development of high-resolution magnetic resonance peripheral nerve imaging[3], including 3D MRN that enables oblique and curved-planar reformations, which are particularly useful for investigating brachial and lumbosacral plexuses and deeply located nerves that are not accessible with ultrasound[4–6].

Diffusion tensor imaging (DTI) is another magnetic resonance technique that in the past decade has been introduced to investigations of peripheral nerve disorders. The technique is sensitive to subtle changes of tissue microstructure and enables measurement of nerve integrity on the basis of quantitative parameters, such as fractional anisotropy, apparent diffusion coefficient, and mean, axial and radial diffusivity[7]. DTI has been used extensively to examine the median nerve at the carpal tunnel and, more recently, to assess the brachial plexus, lumbar plexus and sciatic nerves[8–14], although its full diagnostic value remains to be determined.

In MRN images, healthy nerves appear as isointense or slightly hyperintense; prominent fascicles can have a slightly higher signal intensity than the surrounding perineurial and epineurial tissue, probably owing to the presence of endoneurial fluid[15]. Diseased nerves become hyperintense relative to muscles, and look focally or globally enlarged[16]. Irrespective of the underlying aetiology, the change in signal intensity results from increased water content in the epineurial space as a result of blood–nerve barrier damage, blockade of axoplasmic flow, inflammation and distal Wallerian degeneration[17]. MRN also provides information about muscle denervation, thus enabling the identification of the precise site of the nerve lesion, as described in experimental[18] and clinical studies[19,20]. In the acute phase of muscle denervation, increased signal intensity can be observed as early as 24 h after nerve injury and can last for more than 2 months, representing enlargement of the capillary bed and shift of fluid to the extracellular space. In the subacute phase, a progressive decrease of signal intensity is associated with initial fat replacement, and in the chronic phase, denervated muscles exhibit atrophy and severe fat replacement. These changes that can be observed with MRN precede the earliest EMG findings of denervation, which are not detectable until the second week, so MRN might help to reduce this diagnostic gap.

Ultrasonography

Ultrasonography is another imaging technique that has become usable as a diagnostic tool in the management of peripheral neuropathies owing to technical advances and the development of affordable high-frequency probes. The high spatial resolution of ultrasonographic imaging — currently below 1 mm — enables detailed imaging of nerve morphology (including fascicles, epineurium, perineurium and echotexture) and size, and of the surrounding structures, such as muscles, soft tissues and vessels[21]. Such imaging can provide accurate evaluation of small nerves, such as the digital nerves[22].

The most important measure that ultrasonography can provide, owing to its sensitivity, is the nerve cross-sectional area, which is the area inside the hyperechoic rim of the epineurium, calculated using the ellipse method or — if the nerve does not have an elliptical or circular shape — the tracing method[23]. Another measure that is usually assessed is the ratio between the cross-sectional area of nerve tracts that are involved in the pathological damage and those that are spared[24,25]. For example, in carpal tunnel syndrome, the ratio between the cross-sectional area of median nerve in the wrist (where the nerve is damaged) and forearm (where the nerve is spared) is measured. This ratio is useful because each nerve serves as a control for itself, thereby overcoming the difficulty of determining normal values owing to interindividual variation. Ultrasonography can also be used for the assessment of intraneural vascular flow and elastography. Assessment of intraneural vascular flow is based on Doppler and power Doppler techniques (the latter being particularly effective to show small vessel flow), which enable depiction of the nerve circulatory system[26]. In healthy nerves, vascularization cannot be detected, whereas increased intraneural vascularization can be seen in entrapment[27], inflammatory neuropathies[22] and neurolymphomatosis[28]. The clinical value of intraneural vascular flow is currently under debate. Elastography can be used to assess the stiffness of nerves, although no evidence exists in relation to its value for assessing neuropathy[29,30].

Fat suppression
Magnetic resonance technique used for suppressing the bright signal of fat and improving the visualization of nerves.

Internal fascicular pattern
Degree of visualization of fascicular bundles as distinct entities, with uniform size and signal intensity in intact nerves.

Reformations
Secondary images obtained from 3D datasets with longitudinal display of the nerve course.

Fractional anisotropy
Common diffusion tensor imaging parameter indicating the directional preference of water diffusion within microscopic tissue structures, with physiologically high values in intact peripheral nerves.

Echotexture
Characteristic pattern or structure of tissue layers as seen during ultrasonography.

In ultrasonographic images, healthy nerves appear as cable-like structures that consist of hypoechoic fascicles and hyperechoic surrounding epineurium. On a transverse scan, they have an approximately round shape and a typical honeycomb appearance, with small dark areas (the fascicles) on a hyperechoic background (the perinerium). On a longitudinal scan, they appear as parallel hypoechoic (fascicles) and hyperecoic (perineurium and epineurium) lines.

Imaging of neuropathies

MRN and ultrasonography have proved to provide reliable information for the diagnostic workup of several types of neuropathies, including nerve entrapment syndromes[24,31–33], nontraumatic brachial plexopathies, and hereditary and immune-mediated disorders[25,34]. Each of these categories is discussed below.

Entrapment neuropathies

Nerve entrapment involves two main variables: the container — a rigid space usually shaped by bone and ligaments — and the contents — the nerve, connective tissue, tendons and muscles. Dynamic changes in the volume of the container and its contents during stress-inducing postures, movements and oedema can lead to nerve entrapment; regions close to limb joints are, therefore, predisposed to entrapment syndromes, in which abnormal posture and repetitive movements induce progressive, focal compression. MRN and high-resolution ultrasonography can provide direct anatomical visualization of entrapped nerves, and can sometimes identify the cause of compression.

MRN can reveal abnormalities within the nerve, visible as changes in signal intensity that are often greatest close to the site of entrapment. MRN can also reveal the associated signs of muscle denervation, such as increased signal intensity in the acute–subacute phase, followed by progressive fat infiltration in the chronic phase. With greater severity of neuropathy, proximal nerve enlargement, fascicular hypertrophy and distal flattening can develop and become visible with MRN[32,35].

Ultrasonography has an advantage over MRN in being able to provide a dynamic evaluation of the nerve in a moving joint, which is crucial for nerve entrapment. Typically, ultrasonography of nerve entrapment reveals characteristic fusiform swelling of the nerve that is maximal close to the compression site, where the nerve suddenly flattens (the notch sign). Sometimes, loss of the normal fascicular pattern and a reduction in echogenicity are also observed[33] (FIG. 1).

Carpal tunnel syndrome. Ultrasonography is widely used to investigate compression of the median nerve in the carpal tunnel (FIG. 1), and these studies have provided standard criteria for the diagnosis of all nerve entrapments with ultrasonography[36,37]. One meta-analysis of papers that reported the sensitivity and specificity of ultrasonography from clinical or nerve conduction studies showed that ultrasonography has a sensitivity of 77.6% and a specificity of 86.8% for diagnosis of carpal tunnel syndrome (CTS)[38]. Interestingly, abnormalities in ultrasonographic images have a linear correlation with hand function (for example, fine finger movement) — the larger the nerve cross-sectional area, the greater the impairment — but not with the severity of the symptoms (such as paraesthesias and dysaesthesias)[39]. Nevertheless, evidence-based guidelines state that the median nerve cross-sectional area at the wrist is of value in combination with nerve conduction studies, and can be used as a diagnostic test[36]. Intraneural Doppler sonography might have a role in the diagnosis of CTS, but what this role is remains unclear owing to technical limitations and a lack of standardization in depicting the vasa nervorum as a sign of inflammation[37].

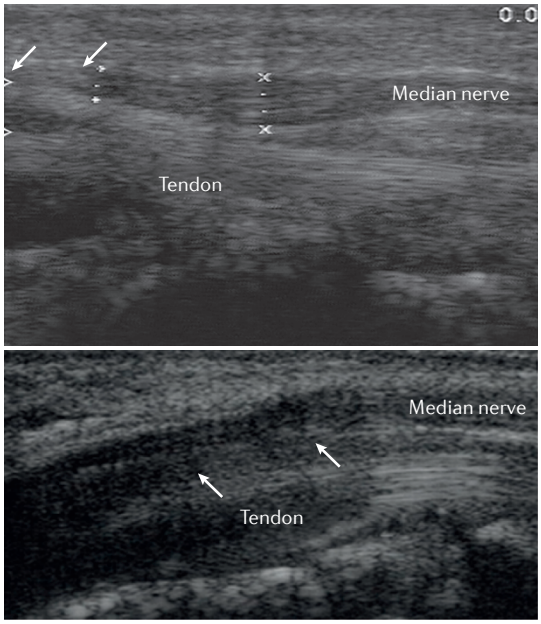

Figure 1 | **Appearance of nerve compression in carpal tunnel syndrome with ultrasonography.** Images are from a 48-year-old female with symptoms of bilateral carpal tunnel syndrome, who had previously had surgery on the right hand with transient partial benefit. Onset of symptoms in the left hand was recent. Ultrasonography of the median nerve in longitudinal view reveals different sites of median nerve compression in each hand. Compression is visible as the notch sign (arrows). Compression is at the distal region of the carpal tunnel, at the capitate bone, in the right hand (top), and in the proximal region of the carpal tunnel at the pisiform level in the left hand (bottom).

The sensitivity of MRN for the diagnosis of CTS has been reported as >90%, in a multicentre prospective study of 120 patients with electrophysiologically confirmed CTS[40]. The length of nerve that appeared abnormal on imaging and the nerve cross-sectional area at the distal radioulnar joint were the best predictors of the severity. Nevertheless, the low specificity of MRN (38%) compared with that of ultrasonography, has limited its use in the management of CTS. However, MRN has a more important role than ultrasonography in the evaluation of atypical CTS, when space-occupying tissue, such as tenosynovitis and ganglion cysts, is suspected or symptoms persist after carpal tunnel release[41].

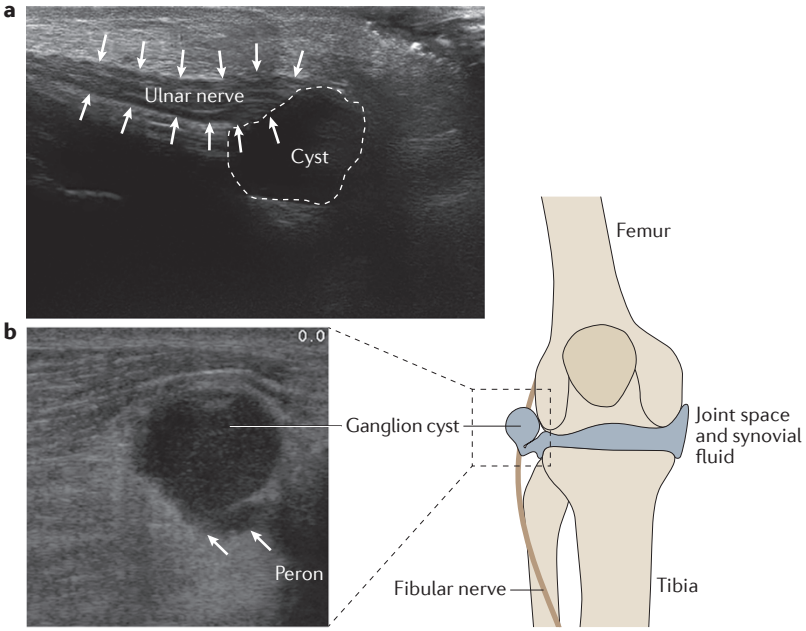

Figure 2 | **Ultrasonography to identify cysts that affect peripheral nerves.** **a** | Ultrasonography examination reveals a synovial cyst (dotted line) that is compressing and dislocating the ulnar nerve (arrows) in the Guyon canal in a 37-year-old man with acute sensory and motor impairment of the ulnar nerve and signs of axonal and demyelinating neuropathy in a nerve conduction study. **b** | In a 48-year-old man with pain in the fibular head region and impaired dorsiflexion of the foot and toe after jogging, ultrasonography revealed a ganglion cyst at the fibular head (arrows) causing axonal damage of fibular nerve and tibialis anterior muscle denervation evident with a nerve conduction study and needle electromyography.

Interest is growing in the use of DTI tractography in the assessment of CTS as a result of evidence for its diagnostic value. A correlation between median DTI metrics and electrophysiology for the carpal tunnel nerve has been reported, suggesting a role for DTI in the *in vivo* assessment of axon and myelin sheath integrity[7,42–44]. According to a meta-analysis published in 2016 that included 316 patients and 293 healthy controls across 12 studies, fractional anisotropy of the median nerve was significantly lower in patients with CTS, and this measure enabled diagnosis of CTS with an overall sensitivity of 82.8% and a specificity of 77.8%[44]. Despite these encouraging preliminary results, DTI of peripheral nerve should still be considered experimental owing to the relatively small datasets in these studies and the variability of DTI thresholds across studies.

Ulnar neuropathy at the elbow. When the ulnar nerve is trapped at the elbow, swelling of the nerve can be detected close to the entrapment site[45,46] (FIG. 2). Use of ultrasonography for dynamic evaluation during flexion and extension of the elbow is crucial for showing luxation and subluxation of the ulnar nerve and modification of the relationship between the nerve and the surrounding structures[47]. As in CTS, assessment of the ratio between cross-sectional areas of ulnar nerve segments that are and are not involved increases the diagnostic yield of ultrasonography, which consequently reaches a sensitivity of 100% and a specificity of 96.7%[48]. The sensitivity of ultrasonography for diagnosis of ulnar nerve entrapment is higher than that of nerve conduction studies[49].

One study has shown that high-resolution 3T MRN can also discriminate between patients with ulnar nerve entrapment at the elbow and healthy controls with high diagnostic accuracy (area under the receiver operating characteristic curve = 0.94). This study used a combined quantitative evaluation of the magnitude and longitudinal extension of the abnormality in the signal intensity from the ulnar nerve. However, more work is required to provide reliable conclusions, as this work was a single prospective study with a small sample size[50].

Other entrapments. MRI and ultrasonography can also be used to diagnose more-complex peripheral nerve conditions. For example, MRI contrast resolution is helpful for the diagnosis of anterior interosseous nerve syndrome — traditionally considered to be a rare entrapment neuropathy — in which high-resolution 3T MRN can identify selective fascicular abnormalities above the entrapment site, suggesting a multifocal mononeuropathy in the majority of cases, as shown by the only study in which this technique was used, which included 24 consecutive patients[51]. The same group obtained similar findings in a series of 19 consecutive patients with posterior interosseous neuropathy syndrome, in which the posterior interosseous nerve is compressed at the supinator muscle in only 16% of cases, whereas partial fascicular lesions of the radial nerve trunk can be detected by 3T MRN at the upper arm level in 84% of cases[52]. Similarly, ultrasonography can be used to depict small nerves and reveal unexpected so-called traumatic entrapment far from the site of a fracture. An example is posterior interosseous nerve syndrome, in which damage has been found to be caused by humeral fracture with radial nerve involvement in 50% of cases[53].

In the lower limbs, the most frequent entrapment neuropathy involves the common fibular nerve, and occurs at the level of the fibular head or in the section of the nerve that extends deep into the origin of the peroneus longus muscle. Common causes of extrinsic compression include crush injury, osteochondroma and aberrant muscles. 3D MRI is particularly useful for the identification of less-common pathological conditions that underlie nerve damage, such as intraneural ganglia that can extend from the proximal tibiofibular joint into the articular branch of the common fibular nerve[54]. Like MRI, ultrasonography can accurately identify intraneural ganglion cysts of the fibular nerve at the fibular head (FIG. 2), as well as other common causes of compression, thus providing information to direct surgical treatment.

Studies have shown that MRI is also useful in the assessment of tibial nerve entrapment. Excellent agreement between high-resolution 3T MRN images and intraoperative findings has been reported for tibial nerve entrapment at the soleal sling, where nerve conduction studies are difficult to perform owing to the depth at which the nerve is located[55]. Similarly, posterior tibial nerve entrapment at the tarsal tunnel, caused by

Luxation
Displacement of the ulnar nerve beyond the tip of the epicondyle during elbow flexion.

ganglion cysts, tenosynovitis, accessory or hypertrophic muscles and foot deformities, can be reliably diagnosed by using MRN[31]. By contrast, the diagnostic role of ultrasonography in tarsal tunnel syndrome remains unclear because it cannot identify definite nerve abnormalities in most cases, probably owing to predominant axonal involvement.

Nontraumatic brachial plexopathies

The brachial plexopathies are diseases of the brachial plexus that, excluding trauma, can occur in several conditions, such as infections, inflammation, radiation therapy, diabetes mellitus or immune-mediated diseases. Owing to its high-contrast resolution and the level of anatomic detail provided, MRN can provide useful information in the diagnostic workup of brachial plexopathies, regardless of aetiology. Evidence for its clinical value is mainly based on case reports and small series[56], but in 2016, a retrospective analysis of 121 studies in which MRN was used to assess inflammatory, traumatic and neoplastic brachial plexopathies reported that clinical opinions were changed by MRN for 75.2% of patients, with substantial changes of opinion for 28% of patients[57], indicating that use of the technology has a meaningful effect on clinical decision-making, so should be used for all assessments of suspected brachial plexopathy. Evidence shows that MRN is useful in brachial plexopathies with a variety of aetiologies. Ultrasonography provides limited information about nontraumatic brachial plexopathies because of blind areas behind the clavicle and within the spine. However, in expert hands, it can be useful for detection of brachial plexus roots, which can appear swollen in inflammatory processes.

In idiopathic neuralgic amyotrophy (INA), acute onset of severe pain usually precedes the development of brachial plexus palsy, and MRN can confirm the clinical diagnosis when performed in the acute to subacute phase, revealing swelling and an increased signal intensity from the proximal brachial plexus (mostly the C5 and C6 nerve roots and the upper trunk) associated with denervation oedema in supraspinatus and infraspinatus muscles[58]. Furthermore, distinguishing INA from cervical spondilogenetic radiculopathy can be challenging, but 3T MRN can detect enlargement of and increased signal intensity from cervical nerve roots, usually without involvement of primary trunks, abnormalities that correlate with spondylotic changes, foraminal stenosis and the distribution of muscle weakness[59,60]. Retrospective unblind studies of ultrasonography in patients with INA have reported different degrees of abnormality in all affected nerves, varying from focal swelling or fascicular enlargement to muscle atrophy; the latter was seen in patients with longer disease duration[61,62].

In the diagnosis of neurogenic thoracic outlet syndrome (TOS), electrophysiological and clinical tests can provide nonspecific findings, such as signs of C8–T1 radiculopathy on needle EMG and pain in the neck, shoulder, arm and hand during arm elevation and abduction, but MRI has been successfully used to gain more-specific insight. For example, MRI can reveal static or dynamic compression of the brachial plexus by structural abnormalities, such as a cervical rib or anomalous first rib, a long C7 transverse process, muscular anomalies or a narrow costoclavicular space[63,64]. According to a prospective study that included 30 patients with a clinical diagnosis of TOS and surgical confirmation of MRI findings[65], the introduction of 3T MRI promises to enable identification of fibrous bands that compress the brachial plexus and cause focal increases in magnetic resonance signal intensity; the study indicated a positive predictive value of 100% for the diagnosis of neurogenic TOS. The contribution of ultrasonography in the diagnosis of TOS is limited, as the technique cannot provide reliable information about nerve abnormalities in the costoclavicular space[66].

In patients with diabetic cervical radiculoplexus neuropathies, MRN can reliably identify abnormalities in the brachial plexus, thereby providing a substantial contribution to the diagnostic workup of the syndrome[67]. Similarly, in radiation plexopathy, which can develop from a few months to many years after radiotherapy, MRN reveals diffuse hypertrophy of the brachial plexus, the extent of which closely correlates with the extent of radiation received, visible as an increase in signal intensity without contrast enhancement[68]. By contrast, neoplastic infiltration of the brachial plexus is characterized by focal or diffuse mass lesion with marked contrast enhancement[69].

Inflammatory and inherited neuropathies

The European Federation of Neurological Societies (EFNS) and Peripheral Nerve Society (PNS) guidelines for the management of chronic inflammatory demyelinating polyradiculoneuropathy (CIDP) recommend that gadolinium enhancement or hypertrophy of the cauda equina, nerve roots or plexuses revealed by MRI are considered to be supportive diagnostic evidence[70]. 3D MRN has provided a further valuable tool for the assessment of the symmetry and variations in signal intensity and size along the course of plexuses and nerve trunks in patients with CIDP[71], and has enabled characterization of some unusual features in patients with atypical CIDP variants. For example, in one study, 3D MRN revealed longitudinal morphological changes from the cervical roots to the nerve trunks of the proximal arm in 88% of patients[72]. 3D MRN can differentiate typical CIDP, in which the distribution of hypertrophy is symmetrical and predominant in the roots with a gradient toward the normalization in the distal nerves, from the multifocal acquired demyelinating sensory and motor neuropathy (MADSAM) variant, in which the hypertrophy is usually asymmetrical and multifocal (FIG. 3).

As in other peripheral nerve diseases, DTI is increasingly being used to detect microstructural abnormalities of nerves in patients with CIDP. Fractional anisotropy can be low in the tibial nerves of patients with various disease durations, and correlates with the amplitudes of compound motor action potentials and, therefore, with the axonal damage[73]. In a selected cohort of patients with CIDP who had disease durations of 1–7 years and had received maintenance therapy with subcutaneous immunoglobulin, MRN did not detect abnormalities of the sciatic nerves, but DTI revealed

Neurogenic thoracic outlet syndrome
Condition resulting from the dynamic compression of the brachial plexus as it travels from the thoracic outlet to the axilla.

low fractional anisotropy that correlated with clinical impairment[74]. This preliminary result suggests that DTI has a role in identifying quantitative measures of microstructural abnormalities in CIDP, although further testing is needed to validate the method.

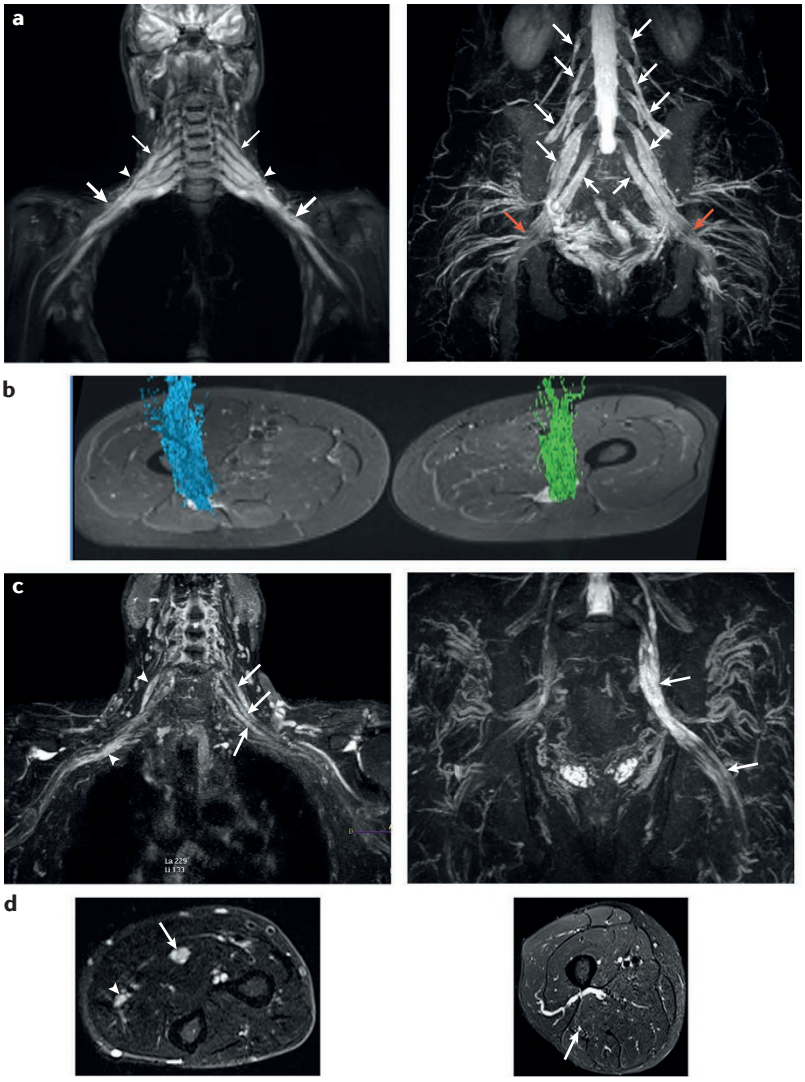

Figure 3 | **3D magnetic resonance neurography and diffusion tensor imaging in immune-mediated neuropathies. a** | The brachial plexus (left) and lumbosacral plexus (right) in a 38-year-old woman with chronic inflammatory demyelinating polyradiculoneuropathy. The images show hyperintensity and symmetrical hypertrophy of the cervical nerve roots (small arrows), primary trunks (arrowheads) and cords (large arrows) in the brachial plexus, and of the L2–S1 spinal roots (white arrows) and sciatic nerves (red arrows) in the lumbosacral plexus. **b** | Diffusion tensor imaging tractography of the right (blue) and left (green) sciatic nerves at the mid-thigh in the same 38-year-old woman, which also appear symmetrically hyperintense and hypertrophic. The mean fractional anisotropy values of both sciatic nerves (0.38) are below the reference values for healthy subjects (0.50). **c** | The brachial plexus (left) and lumbosacral plexus (right) in a 68-year-old man with multifocal acquired demyelinating sensory and motor neuropathy. Arrows indicate typical asymmetrical hypertrophy. In the brachial plexus, arrows show enlargement of the left C5, C6 and C7 nerve roots, and arrowheads show enlargement of the right C5 nerve root and the infraclavear portion of the plexus. In the lumbosacral plexus, arrows indicate enlargement of the left L4, L5 and S1 nerve roots and the sciatic nerve. **d** | Cross sections of the left forearm (left) and the right mid-thigh (right). In the forearm, the arrow indicates enlargement of the median nerve and the arrowhead indicates enlargement of the ulnar nerve. In the thigh, the arrow indicates enlargement of the right sciatic nerve.

The EFNS–PNS guidelines also include MRI findings as supportive criteria for the diagnosis of multifocal motor neuropathy (MMN) and in the differential diagnosis of MMN, CIDP, MADSAM and motor neuron disease[75]. MRI studies have shown that 40–50% of patients with MMN exhibit asymmetrical hypertrophy and abnormalities in signal intensity or contrast-enhancement at the brachial plexus, and the pattern of signal alterations closely correlates with the distribution of muscle weakness[76].

In patients with Charcot–Marie–Tooth disease (CMT), MRN has been used to reveal bilateral hypertrophy of the brachial and lumbosacral plexuses, as well as diffuse symmetrical enlargement of peripheral nerves and/or cauda equina[77,78]. Most peripheral nerves are uniformly affected, and those that are affected are characterized by diffuse fascicular hypertrophy and produce a high MRN signal intensity. The sciatic nerve cross-sectional area, measured at the mid-thigh with MRN, is greater in CMT than in CIDP[79] and can help with the differential diagnosis.

Transthyretin familial amyloid polyneuropathy (TTR-FAP), a rare but life-threatening disease, is the most common form of inherited amyloidosis[80]. Early diagnosis is crucial for initiation of disease-modifying therapies[81], and a study published in 2015 suggests that high-resolution 3T MRN can be used to help with early diagnosis[82]. In this study, MRN was used to identify and quantify the distribution of peripheral nerve injury within the fascicles throughout the length of the sciatic nerves in people with TTR-FAP, and revealed abnormalities even in asymptomatic carriers of the causative gene. These findings suggest that MRN could be used to detect changes that precede the clinical and electrophysiological onset.

The only study in which ultrasonography was used to image nerves in TTR-FAP found a nonspecific pattern of nerve abnormalities[83]. By contrast, evidence suggests that ultrasonography has a role in the assessment of several acquired inflammatory and inherited polyneuropathies[84–87]. A protocol for the differential diagnosis of chronic immune-mediated neuropathies with ultrasonography has been proposed[88]. Characteristic ultrasonography findings in demyelinating neuropathies are enlarged nerve cross-sectional areas, either in focal segments or diffusely, together with abnormalities of nerve and fascicle echogenicity. In acquired inflammatory demyelinating neuropathies, such as CIDP, intra-nerve variability in cross-sectional areas is usually greater[25] — often with most enlargement in the proximal segments of nerve and roots — than in inherited demyelinating neuropathies, such as CMT type 1A, in which enlargement of cross-sectional area is usually uniform along the entire nerve[86,89]. Nevertheless, clinical presentations of CIDP are heterogeneous, and this variation is reflected in a wide range of ultrasonography findings. On the basis of cross-sectional area and echogenicity[87], these findings can be divided into three classes: enlarged and hypoechoic nerves (class 1); enlarged nerves with hypoechoic and hyperechoic fascicles (class 2); and normal-size but hyperechoic nerves

Notalgia
Patchy area of dysaesthesia and altered sensation classically located in the midback skin, but occurring also in other areas of the body.

Ehlers–Danlos syndrome
Condition encompassing various heritable soft connective tissue disorders characterized by joint hypermobility, skin texture abnormalities and visceral and vascular fragility or dysfunctions; six major variants are currently recognized.

(class 3). Evidence suggests that these classes of findings correlate with the course of the disease[87]: class 1 has been reported to correlate with good responses to treatment[90], and class 3 with an increased duration, probably owing to axonal involvement[91]. Ultrasonography has also indicated an increase in nerve vascularization in patients with CIDP[92], although the clinical meaning is uncertain.

In patients with MADSAM, ultrasonography can detect the same asymmetrical and multifocal nerve enlargement as MRN[93]. By contrast, in MMN, ultrasonography can detect enlargement of nerves at sites that are not clinically involved[94], although the enlargement in cross-sectional area has a weak correlation with electrophysiological findings[95]. Nevertheless, ultrasonography might help to differentiate MMN from lower motor neuron disease[96,97], as enlarged nerves or roots are more common in MMN.

Assessment of small-fibre neuropathies

Small-fibre neuropathies (SFNs) are clinical conditions that are characterized by the predominant involvement of somatic unmyelinated C-fibres and thinly myelinated Aδ-fibres that convey thermal and nociceptive stimuli. The most common clinical manifestation is the sensation of burning feet, although focal neuropathies — such as notalgia[98] and burning mouth[99] — and diffuse pain have been described and suggest the involvement of primary sensory neurons[100,101]. Primary involvement of the autonomic system means that small nerve fibres with autonomic functions are predominantly impaired rather than small fibres with somatic functions. In typical painful SFNs, patients can report autonomic symptoms; in this case, skin cholinergic and vasomotor fibre dysfunction occur more frequently than does systemic adrenergic involvement, which explains the observation that skin vascular deregulation in the lower limbs occurs more frequently than systemic cardiovascular dysautonomia[102].

Conclusive studies are needed to determine the epidemiology of SFN, but it is prevalent among patients with diabetes mellitus, impaired glucose tolerance, and connective tissue disorders[103]. SFN has also been identified as an adverse effect of rapid glycaemic correction in diabetes mellitus; this condition was previously known as insulin neuritis[104].

SFN is also associated with a widening spectrum of systemic diseases; the most recent disease to be associated, in 2016, is Ehlers–Danlos syndrome[105]. In many patients, SFN is idiopathic, but pathogenic mutations in genes that encode for various sodium channels have been identified in some patients[106–108]. A correlation between specific mutations and painful and autonomic symptoms has been reported[109], and novel mutations in *COL6A5* have been found in patients with neurogenic itch and SFN[110].

The diagnostic criteria for SFN have been revised[111,112] to provide a grading based on symptoms, signs and findings from validated examination. A diagnosis of 'possible' SFN is indicated by length-dependent symptoms and/or clinical signs of small-fibre damage. A diagnosis of 'probable' SFN is indicated by length-dependent symptoms, clinical signs of small-fibre damage, and normal sural nerve conduction studies. Finally, a diagnosis of 'definite' SFN is indicated by length-dependent symptoms, clinical signs of small-fibre damage, normal sural nerve conduction studies, altered intraepidermal nerve fibre (IENF) density at the ankle and/or abnormal quantitative sensory testing (QST; BOX 1) thermal thresholds at the foot. These criteria have been proposed for diabetic SFN, but can be applied to all patients with suspected SFN, irrespective of the associated disease or condition.

The MRI and ultrasonography techniques discussed above cannot be used in the assessment of small-nerve fibres owing to resolution limitations that prevent identification of these fibres in the skin and in the Remak bundles, in which they run into the sensory nerves. Until approximately 15 years ago, the only technique available to support a clinical diagnosis of SFN was QST, the automated assessment of thermal thresholds[113,114] (BOX 1). The introduction of skin biopsies, however, has enabled more reliable diagnosis through quantification of IENFs to assess for degeneration. Now, several other techniques are emerging that hold promise for the assessment of small-fibre neuropathies, but are currently used mainly in clinical research settings — these technologies include corneal confocal microscopy, nociceptive evoked potentials and microneurography.

Skin biopsy

Analysis of skin biopsy samples entered the neurologists' diagnostic toolbox as a result of the development of antibodies against ubiquitin carboxyl-terminal hydrolase

Box 1 | **Quantitative sensory testing**

Automated assessment of thermal thresholds was the first tool used to support a clinical diagnosis of small-fibre neuropathy (SFN)[113,114]. Quantitative sensory testing (QST) is based on the psychophysical examination of sensory nerve fibre functions through assessment of thresholds to various stimuli, including pressure, vibration, cold, warmth, heat, cold pain and heat pain. This approach enables identification of gain-of-function phenomena, such as allodynia and hyperalgesia.

QST is widely used and considered to be useful for the diagnosis of SFN[102,204,205], but the approach has several drawbacks that limit its reliability for identification of SNF in individuals and might make it more useful in population studies[206,207]. For example, QST requires alert and cooperative patients, and can be influenced by malingering or psychogenic conditions[207–209]. The major limitation, however, is a lack of specificity. For example, in a study of sensory abnormalities in neuropathic pain, QST in 1,236 patients revealed remarkable phenotypic heterogeneity, resulting in overlap between CNS diseases (for example, stroke and multiple sclerosis) and peripheral neuropathies[210]. In another study, comparison of QST thresholds in patients with and without pain after traumatic nerve injury revealed no difference in thermal, mechanical and pain sensitivity besides a higher frequency of allodynia in the group with pain.

In the past few decades, more than 15 different methodological approaches to QST have been developed[207,211,212], thereby limiting the possibility of a standardized assessment. The International Association for the Study of Pain has provided consensus criteria on use and interpretation of QST findings[213], emphasizing that a standardized protocol, adequate equipment, trained personnel and use of standard reference values should be developed.

Some studies in which thermal and pain thresholds have been compared with skin biopsy findings have demonstrated a correlation between cold and/or warm thresholds and IENF density[164,214–217], but other similar studies have not[218–220]. These findings suggest that QST should be considered as an additional diagnostic test for SFN, but alongside a well-characterized clinical assessment and a skin biopsy[206].

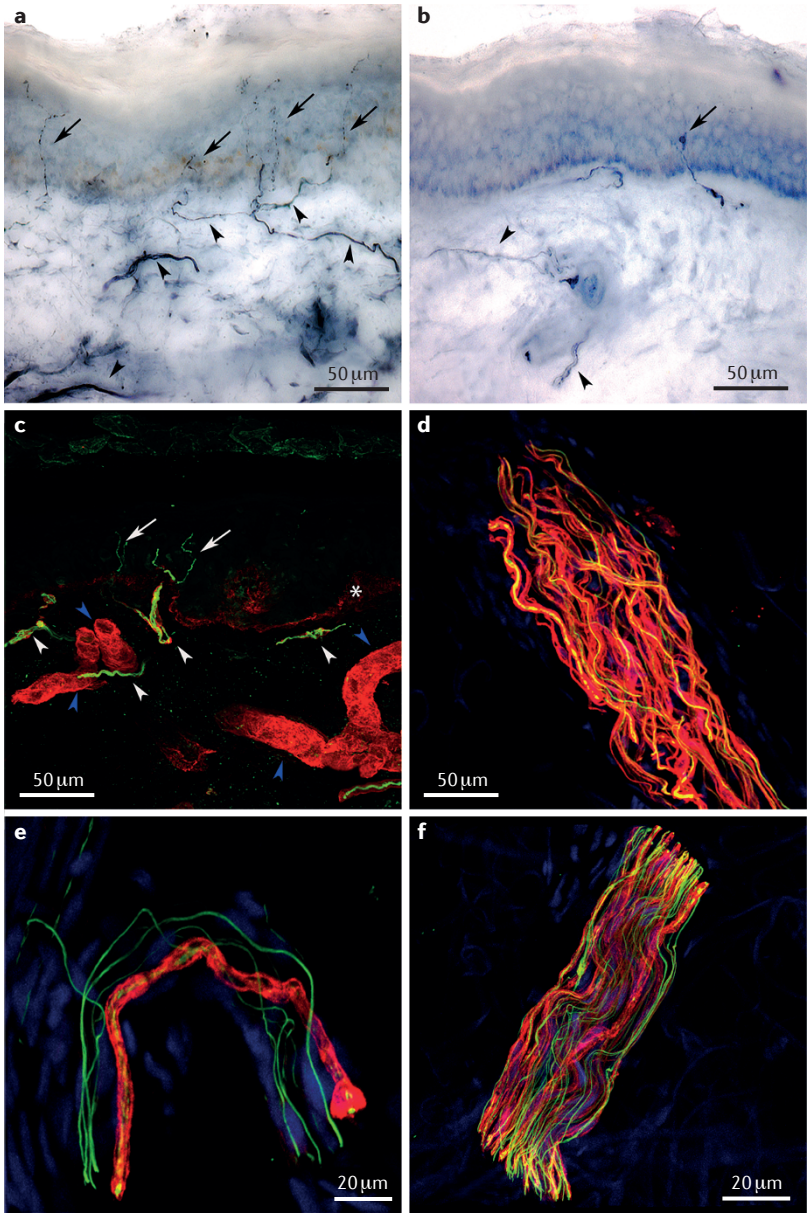

Figure 4 | **Representative images of skin biopsy sample sections using different techniques and antibodies that target different structures.** **a** | Bright-field immunohistochemistry with anti-PGP9.5 antibody staining in a healthy biopsy sample. Staining reveals the density of dermal (arrowheads) and intraepidermal (arrows) nerve fibres. **b** | Anti-PGP9.5 antibody staining of a biopsy sample from a patient with small-fibre neuropathy shows reduced density of dermal (arrowheads) and intraepidermal (arrows) nerve fibres. **c** | Indirect confocal microscope double staining immunofluorescence using anti-PGP9.5 antibody in a healthy individual shows dermal (white arrowheads) and intraepidermal (arrows) nerve fibres, and anti-collagen IV antibody shows the dermal–epidermal junction (asterisk) and vessels (blue arrowheads). **d** | Indirect confocal microscope triple staining immunofluorescence using anti-myelin basic protein antibodies (red) and anti-PGP9.5 antibodies (green), showing normal myelin sheath and axons in a dermal bundle. **e** | Indirect confocal microscope triple staining immunofluorescence using anti-S100 myelin antibody (red) and anti-neurofilament antibodies (green) to show normal Schwann cells in a dermal nerve bundle. **f** | Indirect confocal microscope triple staining immunofluorescence using anti-S100 myelin antibody (red) and anti-neurofilament antibodies (green) to show cytoskeleton in a dermal nerve bundle. Myelin and axon staining merge to yellow. In parts **d–f**, DAPI staining of surrounding fibroblasts is shown in blue.

isozyme L1 (UCH-L1, also known as PGP9.5) a diffusely distributed neuronal ubiquitin carboxyl-terminal hydrolase transported by the slow component of axonal transport[98]. PGP9.5 is a nonspecific cytoplasmic panaxonal marker that enables reliable identification of dermal nerve fibres and IENFs[115] via bright-field immunohistochemistry or indirect immunofluorescence (FIG. 4). IENFs have exclusive somatic functions and widely express the capsaicin receptor, making them the most distal nociceptors[116], and their degeneration has been observed in several systemic illnesses, including neurodegenerative diseases, and associated with mutations in genes that encode sodium channels[103].

Before the development of anti-PGP9.5 antibodies, visualization of unmyelinated C-fibres and thinly myelinated Aδ-fibres required analysis of a nerve biopsy with electron microscopy. The availability of skin biopsy prompted the recognition of SFN as a distinct clinical entity[117]. Furthermore, skin biopsy has enabled investigation of the innervation of autonomic structures, such as sweat glands, hair follicles and arteriovenous anastomosis, in autonomic neuropathies[118–120].

Following the pioneering studies that introduced skin biopsies[121–123], a study was conducted to establish reference ranges for nerve fibre density, but participants were not stratified by age or sex[124]. The limitations of this study have probably led to overestimations of the prevalence of SFN, even when the condition is associated with typical risk factors, such as diabetes mellitus and impaired glucose tolerance. Only in the past few years have reference studies provided adjusted reference values for bright-field immunohistochemistry[125] and indirect immunofluorescence[126] techniques that are suitable for clinical use. These studies demonstrated that IENF density decreases with increasing age, and enable diagnosis of SFN when nerve fibre density is in the lowest 5th percentile[125,126]. Reference values of IENF density in children are also available[127]. Guidelines for the use of skin biopsy in clinical practice have been published[128], providing standardization of the technical procedures, including IENF count, worldwide.

A study published in 2015 compared the diagnostic capabilities of bright-field immunohistochemistry and indirect immunofluorescence on the basis of reference values, and demonstrated a high level of agreement between the techniques, suggesting that they have comparable validities[129]. Other work has shown that in healthy individuals and patients with SFN, the IENF density is consistent between the two legs of an individual, either healthy or affected by SFN, and that the density does not change within 3 weeks, the mean period of epidermal renewal[130]. This finding indicates that skin biopsy could be used as an outcome measure in clinical trials of neuroregenerative treatments. In 2015, an innovative semi-automated method for quantifying IENFs in skin biopsy samples proved to have high reproducibility[131]. This approach could increase the speed of sample processing, although the reproducibility is higher for immunofluorescence than for the bright-field technique.

Skin biopsy also enables reliable quantification of the density of subepidermal nerve fibres[132]. The technique is more complex and time-consuming than that

for quantification of IENFs. Nevertheless, the available evidence suggests that the new method, which is based on the unbiased measurements of the overall length of all dermal fibres using the bright-field technique, can consistently distinguish healthy individuals from patients with SFN[132]. In one study, analysis of the density of parts of the subepidermal nerve plexus with immunofluorescence — when associated with the quantification of IENF density — improved the sensitivity of skin biopsy for diagnosis of SFN[133]. In another study, internode length and internodal gap length of myelinated dermal nerve fibres were quantified and combined with the findings of nerve biopsy, and suggested that the fibres are thin endings of large myelinated Aβ fibres[134]. The same group used this approach to investigate patients with CMT, and demonstrated similar internodal shortening associated with different causal mutations, and a wider nodal gap in the CMT type 1A, providing insight into their role in determining changes of conduction velocity[135,136].

Quantitative analysis of the nerve fibres that innervate the autonomic organs of the skin is particularly complex because of the 3D structures of these organs. Stereological methods have been used to determine the morphometry of sweat gland and pilomotor muscle innervation, showing a correlation between the innervation density and the dysautonomic symptoms experienced by patients with diabetic neuropathy[119,137]. Studies have also shown that skin biopsy can not only provide structural and pathological evidence of nerve degeneration, but also provide surrogate markers of function, thereby widening the applications of skin biopsy in assessing the involvement of the peripheral autonomic system and as a potential outcome measure in clinical trials. For example, reductions in sudomotor innervation correlated with autonomic symptoms, progressive disability and reduced performance in autonomic functional tests in 28 patients with familial amyloid neuropathy[138]. In 97 patients with diabetic neuropathy, innervation of sweat glands correlated with glycated haemoglobin and BMI[139]. Similarly, degeneration of cholinergic fibres that innervate the sweat glands has been identified in the anhidrotic skin areas of patients with Ross syndrome[140]. This change, along with severe heat intolerance owing to the inability to sweat, could be used to distinguish patients with Ross syndrome from those with Holmes–Adie syndrome, who also exhibit sweating abnormalities[141]. The pathological abnormalities in patients with Ross syndrome were found to also involve the noradrenergic fibres that innervate arrector pilorum muscles and vessels, and, to a lesser extent, somatic unmyelinated and myelinated nerve fibres[141]. Skin biopsies have also been used to examine autonomic innervation in multiple system atrophy. A study of three patients with multiple system atrophy found that innervation of sweat glands in the anhidrotic skin areas of these patients was intact, suggesting that the impairment is preganglionic[142], although this finding was not confirmed by a subsequent study with a larger cohort of patients, in whom diffuse degeneration of sudomotor nerve fibres was observed[143].

Beyond classic SFNs, skin biopsy can be used to identify small-fibre pathology in painless neurodegenerative disorders, such as Parkinson disease (PD)[144,145] and amyotrophic lateral sclerosis (ALS)[146–148]. Evidence shows that patients with PD exhibit a marked loss of IENFs and Meissner corpuscles that accompanies abnormal tactile, thermal and mechanical pain perception[144]. The epidermal denervation has been confirmed in another study[145], which also identified a correlation between deposits of phosphorylated α-synuclein in sensory and autonomic nerve fibres and the pattern of dermal nerve fibre loss. Together, these findings suggest that small-fibre pathology is intrinsic to PD and that the detection of phosphorylated α-synuclein in dermal nerve fibres might serve as a diagnostic test with high specificity and low sensitivity. Similarly, further studies have demonstrated that up to 75% of patients with ALS have small-fibre pathology, evident as a decreased density of IENFs[148], and exhibit asymptomatic involvement of autonomic nerves and Meissner corpuscles[147]. One study suggested that loss of IENFs was only seen in patients with spinal-onset ALS[149], but a larger study that included patients with sporadic and genetic ALS found no correlations between phenotype, genotype and disease course[148]. A 2016 study in a mouse model of ALS demonstrated degeneration of small nerve fibres in these animals, as revealed by skin biopsy; this degeneration resulted from a specific susceptibility of small primary sensory neurons caused by the accumulation of a toxic splicing variant of peripherin that leads to altered neurofilament assembly[150].

Dermal innervation is mainly provided by myelinated nerves, so skin biopsy offers a window for examining patients with inflammatory neuropathies. Although skin biopsy is not expected to have a major role in diagnosing specific immune-mediated neuropathies[151], it does enable some features of myelinated nerves to be examined over time using a minimally invasive and repeatable technique. For example, skin biopsy was used to reveal specific IgM deposits in patients with anti-myelin-associated glycoprotein neuropathy[152,153] and early disruption of myelinated nerves in patients with Guillain–Barré syndrome[154].

Corneal confocal microscopy

The cornea is highly innervated by small nerve fibres of trigeminal origin that enter through the middle third of the stroma[155,156]. These fibres can be visualized and quantified by using *in vivo* corneal confocal microscopy, a noninvasive technique that rapidly evolved from a research technique to an emerging clinical tool[157]. Development of automated corneal nerve image analysis[158–161] and, most importantly, the establishment of reference values[162] have made corneal confocal microscopy a new and reliable diagnostic tool for SFN. The exact role of the technique in the diagnosis of individual patients with suspected SFN in clinical practice, however, remains to be determined, and requires further studies in future.

To date, corneal confocal microscopy has predominantly been used to assess patients with diabetes mellitus[163–166], but the technique has also been used to

Ross syndrome
Rare clinical disorder of unknown cause characterized by the triad of tonic pupil, hyporeflexia and segmental anhidrosis.

Holmes–Adie syndrome
Rare clinical disorder of unknown cause characterized by tonic pupil and hyporeflexia, with normal sweating function.

Stroma
Layer of the cornea located behind the Bowman layer and in front of the Descemet membrane, representing ~90% of the total corneal thickness and giving the cornea its strength.

demonstrate small-fibre involvement in several other conditions, including CMT type 1A[167], hereditary sensory and autonomic neuropathy[168], Fabry disease[169], autoimmune neuropathy[170] and chemotherapy-induced neuropathy[171]. As with skin biopsy, with which its agreement in a recent comparative study was good[172], corneal confocal microscopy provided evidence of nerve fibre regeneration in patients with diabetes mellitus[173] and after pancreas transplantation[174,175], suggesting a potential use as an outcome measure in clinical trials.

Small-fibre-related evoked potentials

The conduction properties of small nerve fibres can be investigated by analysing evoked potentials in response to stimuli that activate the nociceptive pathway[176]. Laser-evoked potentials and contact heat-evoked potentials are based on activation of Aδ-fibres and C-fibres, although seem to have limited clinical applicability. Pain-related evoked potentials are based on preferential electrical stimulation of Aδ-fibres[177], and intraepidermal electrical stimulation has been developed most recently to provide functional information about Aδ-fibres and C-fibres[178,179]. Pain-related evoked potentials seem to hold some promise for clinical evaluation of SFNs.

Laser-evoked potentials. Laser-evoked potentials can be induced with stimulation from solid-state (thulium or neodinium-based) or CO_2 lasers. Solid-state lasers use shorter wavelengths, which leads to a faster rise in temperature that means shorter pulses and higher amplitudes are needed, thereby shortening the latency of the cortical response and reducing the risk of superficial burns[180]. However, the shorter wavelength means the technique is more easily affected by skin pigmentation than use of CO_2 lasers, so that the delivery of energy to the skin is uneven. Laser stimulation causes a pricking sensation as a result of Aδ-fibre activation, and a diffuse burning sensation owing to activation of C-fibres. The main laser-evoked potential signal is a large negative–positive complex with a latency of 150–380 ms (REF. 181). An earlier and smaller negative wave with a latency of 150–180 ms is detected at the temporal regions and is less affected by the patient's attention than the earlier signal, providing an advantage in terms of the reliability of the signal and, therefore, the definition of the abnormal responses in the clinical setting[181,182]. Specific techniques can be used to elicit ultra-late potentials with latencies of 750–1200 ms that are related to activation of C-fibres[183–186]. Abnormal laser-evoked potential latency indicates conduction abnormalities in the thermal nociceptive pathway, which includes peripheral nerves, plexus, roots, spinal cord and brainstem[181]. The site of damage is impossible to identify, so laser-evoked potentials cannot be used for the diagnosis of SFNs, but are useful for studying the function and modulation of the thermal nociceptive pathway.

Contact heat-evoked potentials. Contact heat-evoked potentials are induced by stimulation of the skin with a heat-foil contact stimulator that heats at 70 °C per second[187] and mechanically activates a larger surface area than that stimulated to evoke laser-evoked potentials[188]. The stimulus can be easily controlled[187,189], and the risk of skin irritation is lower than with lasers[190]. Contact heat-evoked potentials enable recording of late and ultra-late potentials associated with activation of Aδ-fibres and C-fibres, respectively[187,191]. Standard reference values were published in 2014 (REF. 192), but this technique has the same limitations as laser-evoked potentials because the site of damage cannot be identified.

Pain-related evoked potentials

Pain-related evoked potentials are induced by electrical stimulation of the skin at the threshold at which the subject feels the stimulus as painful[177]. Stimulation is delivered via a concentric planar electrode and is limited to the superficial layer of the dermis. A pushpin-like electrode with a length of 0.2 mm can be used for intraepidermal stimulation. Pain-related evoked potentials reflect early depolarization of superficial Aδ-fibres; deeper, non-nociceptive skin fibres are not activated[177]. Some evidence suggests that altered pain-related evoked potentials correlate with low IENF density in patients with HIV-related SFN[193], and that abnormal pain-related evoked potentials can aid early diagnosis of diabetic neuropathy[194]. Furthermore, standard reference values were published in 2015 (REF. 195), and further work is now needed to determine whether pain-related evoked potentials have clinical value in the diagnosis of small-fibre neuropathies.

Microneurography

Microneurography involves using a microelectrode to record nerve activity in a superficial nerve upon stimulation of its cutaneous receptive field. The signals recorded reflect action potentials elicited by single axons[196]. The technique enables the recording of several parameters, including the conduction velocity of myelinated and unmyelinated fibres and changes in their onset latency related to activity-dependent slowing of conduction velocity, a physiological property of unmyelinated C-fibres.

Microneurography is used to investigate spontaneous and induced activity of sensory nerve fibres, enabling a measure of positive (for example burning pain, paroxysmal pain, paraesthesia and allodynia) and negative phenomena (for example loss of thermal and nociceptive sensation)[196], and has provided insight into the physiology of nociceptors and the mechanisms underlying their sensitization[197–200]. The technique enables identification of different profiles of neural activity that correspond to functionally distinct subpopulations of sensory and sympathetic neurons[201]. Spontaneous ongoing discharges of C-nociceptors are considered to be pathological causes of pain, and microneurography has been used to demonstrate that such spontaneous discharge is present in patients in whom pain is associated with SFN[200]. The same technique has been used to reveal spontaneous discharge of C-nociceptors in fibromyalgia[200,202,203], thereby widening the spectrum of disorders that have been related to SFN.

The use of microneurography in routine clinical practice is limited by the need for specifically trained operators, the duration of the examination and the complexity of interpreting the data, but the information provided can reveal impairment of different subtypes of somatic and autonomic small-nerve fibres and give insight into the pathophysiology of symptoms.

Conclusions

MRN and ultrasonography are increasingly being used in the diagnostic workup of peripheral neuropathies as techniques that complement neurophysiology. Both MRN and ultrasonography provide direct visualization of nerve lesions, accurate anatomical localization and the distribution of disease along the nerve trunks. By contrast, nerve conduction studies and electromyography have intrinsic limitations in identifying the lesion site and the aetiology of the underlying nerve damage.

MRN and ultrasonography each offer distinct advantages. MRN has a higher contrast resolution and sensitivity to blood–nerve barrier disruption than does ultrasonography, enabling better characterization of neuropathies, identification of muscle denervation, visualization of brachial and lumbosacral plexuses and deeply situated nerves, and the quantitative evaluation of nerve microstructural integrity. By contrast, ultrasonography offers higher spatial resolution than MRN, which enables the detection of abnormalities in thin nerves at the distal extremities, the assessment of long nerve segments in a single study. Ultrasonography also offers the opportunity to perform dynamic studies, and the time effectiveness, lower cost, wider availability, and easier technique of examination.

Currently, ultrasonography is the preferred imaging technique for routine investigation of peripheral nerve diseases owing to its widespread availability, relatively low costs, and the possibility of using the technique in combination with nerve conduction studies. MRN should be reserved for the exploration of anatomical sites that are not easily accessible with ultrasonography, and for patients in whom ultrasonography and electrophysiology are inconclusive. A combination of ultrasonography and MRN is particularly useful for investigating atypical or complex polyneuropathies, in which the two techniques provide complementary information.

In the growing field of SFNs, where traditional nerve conduction studies are of little or no help, and the traditional approach of quantitative sensory testing is unreliable, skin biopsy has become established as crucial for making a reliable diagnosis. The advantage of skin biopsy is that it provides direct evidence for the loss of small-nerve fibres and can reveal progressive degeneration or regeneration. As the technique is minimally invasive and rarely associated with adverse effects when appropriately managed with sterile technique and care, skin biopsy can be repeated so as to follow-up the course of the neuropathy. Moreover, skin biopsy can be performed in any affected area to diagnose mononeuropathies or to correlate symptoms with small nerve fibre loss in patients with diffuse pain syndromes. Skin biopsy cannot determine the aetiology of the neuropathy, although it can be used to investigate dermal myelinated nerve fibres to determine changes that are specifically associated with acquired or genetic neuropathies.

Other techniques can provide evidence of structural or functional impairment of small-nerve fibres. Corneal confocal microscopy can reliably assess the *in vivo* density and length of trigeminal small-nerve fibres in neuropathies of different aetiology, and the availability of reference values can support the diagnosis of SFN in a clinical setting. Functional involvement of small-nerve fibres and the correlation of this involvement with pathology can be assessed with specific neurophysiological techniques, such as small-fibre-related evoked potentials and microneurography, which have a limited role in the routine clinical setting but can provide information about the impairment of the nociceptive pathway and specific subtypes of small-nerve fibres, respectively.

1. Watson, J. C. & Dyck, P. J. Peripheral neuropathy: a practical approach to diagnosis and symptom management. *Mayo Clin. Proc.* **90**, 940–951 (2015).
2. Filler, A. G. *et al.* Magnetic resonance neurography. *Lancet* **341**, 659–661 (1993).
3. Thawait, S. K. *et al.* High-resolution MR neurography of diffuse peripheral nerve lesions. *AJNR Am. J. Neuroradiol.* **32**, 1365–1372 (2011).
4. Vargas, M. I. *et al.* New approaches in imaging of the brachial plexus. *Eur. J. Radiol.* **74**, 403–410 (2010).
5. Viallon, M., Vargas, M. I., Jlassi, H., Lovblad, K. O. & Delavelle, J. High-resolution and functional magnetic resonance imaging of the brachial plexus using an isotropic 3D T2 STIR (Short Term Inversion Recovery) SPACE sequence and diffusion tensor imaging. *Eur. Radiol.* **18**, 1018–1023 (2008).
6. Chhabra, A. *et al.* MR neurography: past, present, and future. *AJR Am. J. Roentgenol.* **197**, 583–591 (2011).
7. Guggenberger, R. *et al.* Assessment of median nerve with MR neurography by using diffusion-tensor imaging: normative and pathologic diffusion values. *Radiology* **265**, 194–203 (2012).
8. Brienza, M. *et al.* 3T diffusion tensor imaging and electroneurography of peripheral nerve: a morphofunctional analysis in carpal tunnel syndrome. *J. Neuroradiol.* **41**, 124–130 (2014).
9. Chhabra, A. *et al.* Anatomic MR imaging and functional diffusion tensor imaging of peripheral nerve tumors and tumorlike conditions. *AJNR Am. J. Neuroradiol.* **34**, 802–807 (2013).
10. Gasparotti, R. *et al.* Feasibility of diffusion tensor tractography of brachial plexus injuries at 1.5 T. *Invest. Radiol.* **48**, 104–112 (2013).
11. Jengojan, S. *et al.* Acute radial nerve entrapment at the spiral groove: detection by DTI-based neurography. *Eur. Radiol.* **25**, 1678–1683 (2015).
12. Kasprian, G. *et al.* Peripheral nerve tractography in soft tissue tumors: a preliminary 3-tesla diffusion tensor magnetic resonance imaging study. *Muscle Nerve* **51**, 338–345 (2015).
13. Ohana, M. *et al.* 3T tractography of the median nerve: optimisation of acquisition parameters and normative diffusion values. *Diagn. Interv. Imaging* **93**, 775–784 (2012).
14. Simon, N. G. *et al.* High-resolution ultrasonography and diffusion tensor tractography map normal nerve fascicles in relation to schwannoma tissue prior to resection. *J. Neurosurg.* **120**, 1113–1117 (2014).
15. Mizisin, A. P. & Weerasuriya, A. Homeostatic regulation of the endoneurial microenvironment during development, aging and in response to trauma, disease and toxic insult. *Acta Neuropathol.* **121**, 291–312 (2011).
16. Aagaard, B. D., Maravilla, K. R. & Kliot, M. Magnetic resonance neurography: magnetic resonance imaging of peripheral nerves. *Neuroimaging Clin. N. Am.* **11**, 131–146 (2001).
17. Stoll, G., Bendszus, M., Perez, J. & Pham, M. Magnetic resonance imaging of the peripheral nervous system. *J. Neurol.* **256**, 1043–1051 (2009).
18. Bendszus, M., Koltzenburg, M., Wessig, C. & Solymosi, L. Sequential MR imaging of denervated muscle: experimental study. *AJNR Am. J. Neuroradiol.* **23**, 1427–1431 (2002).
19. Bendszus, M. *et al.* MR imaging in the differential diagnosis of neurogenic foot drop. *AJNR Am. J. Neuroradiol.* **24**, 1283–1289 (2003).
20. Kim, S. J. *et al.* MR imaging mapping of skeletal muscle denervation in entrapment and compressive neuropathies. *Radiographics* **31**, 319–332 (2011).
21. Martinoli, C. *et al.* Ultrasound of tendons and nerves. *Eur. Radiol.* **12**, 44–55 (2002).
22. Gallardo, E., Noto, Y. & Simon, N. G. Ultrasound in the diagnosis of peripheral neuropathy: structure meets function in the neuromuscular clinic. *J. Neurol. Neurosurg. Psychiatry* **86**, 1066–1074 (2015).
23. Patel, P., Norbury, J. W. & Fang, X. Sonographic measurements of the ulnar nerve at the elbow with different degrees of elbow flexion. *PM R* **6**, 395–399 (2014).
24. Hobson-Webb, L. D., Massey, J. M., Juel, V. C. & Sanders, D. B. The ultrasonographic wrist-to-forearm median nerve area ratio in carpal tunnel syndrome. *Clin. Neurophysiol.* **119**, 1353–1357 (2008).

25. Padua, L. *et al.* Intra- and internerve cross-sectional area variability: new ultrasound measures. *Muscle Nerve* **45**, 730–733 (2012).
26. Borire, A. A. *et al.* Utility of maximum perfusion sity as an ultrasonographic marker of intraneural blood flow. *Muscle Nerve* **55**, 77–83 (2017).
27. Frijlink, D. W., Brekelmans, G. J. & Visser, L. H. Increased nerve vascularization detected by color Doppler sonography in patients with ulnar neuropathy at the elbow indicates axonal damage. *Muscle Nerve* **47**, 188–193 (2013).
28. Vijayan, J., Chan, Y. C., Therimadasamy, A. & Wilder-Smith, E. P. Role of combined B-mode and Doppler sonography in evaluating neurolymphomatosis. *Neurology* **85**, 752–755 (2015).
29. Martin, M. J. & Cartwright, M. S. A pilot study of strain elastography in the diagnosis of carpal tunnel syndrome. *J. Clin. Neurophysiol.* http://dx.doi.org/10.1097/WNP.0000000000000334 (2016).
30. Greening, J. & Dilley, A. Posture-induced changes in peripheral nerve stiffness measured by ultrasound shear-wave elastography. *Muscle Nerve* **55**, 213–222 (2017).
31. Donovan, A., Rosenberg, Z. S. & Cavalcanti, C. F. MR imaging of entrapment neuropathies of the lower extremity. Part 2. The knee, leg, ankle, and foot. *Radiographics* **30**, 1001–1019 (2010).
32. Petchprapa, C. N. *et al.* MR imaging of entrapment neuropathies of the lower extremity. Part 1. The pelvis and hip. *Radiographics* **30**, 983–1000 (2010).
33. Cartwright, M. S. & Walker, F. O. Neuromuscular ultrasound in common entrapment neuropathies. *Muscle Nerve* **48**, 696–704 (2013).
34. Trivedi, J. R., Phillips, L. & Chhabra, A. Hereditary and acquired polyneuropathy conditions of the peripheral nerves: clinical considerations and MR neurography imaging. *Semin. Musculoskelet. Radiol.* **19**, 130–136 (2015).
35. Chhabra, A. Peripheral MR neurography: approach to interpretation. *Neuroimaging Clin. N. Am.* **24**, 79–89 (2014).
36. Cartwright, M. S. *et al.* Evidence-based guideline: neuromuscular ultrasound for the diagnosis of carpal tunnel syndrome. *Muscle Nerve* **46**, 287–293 (2012).
37. Vanderschueren, G. A., Meys, V. E. & Beekman, R. Doppler sonography for the diagnosis of carpal tunnel syndrome: a critical review. *Muscle Nerve* **50**, 159–163 (2014).
38. Fowler, J. R., Gaughan, J. P. & Ilyas, A. M. The sensitivity and specificity of ultrasound for the diagnosis of carpal tunnel syndrome: a meta-analysis. *Clin. Orthop. Relat. Res.* **469**, 1089–1094 (2011).
39. Padua, L. *et al.* Carpal tunnel syndrome: ultrasound, neurophysiology, clinical and patient-oriented assessment. *Clin. Neurophysiol.* **119**, 2064–2069 (2008).
40. Jarvik, J. G. *et al.* MR nerve imaging in a prospective cohort of patients with suspected carpal tunnel syndrome. *Neurology* **58**, 1597–1602 (2002).
41. Campagna, R. *et al.* MRI assessment of recurrent carpal tunnel syndrome after open surgical release of the median nerve. *AJR Am. J. Roentgenol.* **193**, 644–650 (2009).
42. Heckel, A. *et al.* Peripheral nerve diffusion tensor imaging: assessment of axon and myelin sheath integrity. *PLoS ONE* **10**, e0130833 (2015).
43. Koh, S. H. *et al.* A comparison of the performance of anatomical MRI and DTI in diagnosing carpal tunnel syndrome. *Eur. J. Radiol.* **83**, 2065–2073 (2014).
44. Wang, H., Ma, J., Zhao, L., Wang, Y. & Jia, X. Utility of MRI diffusion tensor imaging in carpal tunnel syndrome: a meta-analysis. *Med. Sci. Monit.* **22**, 736–742 (2016).
45. Omejec, G., Zgur, T. & Podnar, S. Diagnostic accuracy of ultrasonographic and nerve conduction studies in ulnar neuropathy at the elbow. *Clin. Neurophysiol.* **126**, 1797–1804 (2015).
46. Bayrak, A. O., Bayrak, I. K., Turker, H., Elmali, M. & Nural, M. S. Ultrasonography in patients with ulnar neuropathy at the elbow: comparison of cross-sectional area and swelling ratio with electrophysiological severity. *Muscle Nerve* **41**, 661–666 (2010).
47. Okamoto, M., Abe, M., Shirai, H. & Ueda, N. Morphology and dynamics of the ulnar nerve in the cubital tunnel. Observation by ultrasonography. *J. Hand Surg. Br.* **25**, 85–89 (2000).
48. Yoon, J. S., Walker, F. O. & Cartwright, M. S. Ultrasonographic swelling ratio in the diagnosis of ulnar neuropathy at the elbow. *Muscle Nerve* **38**, 1231–1235 (2008).
49. Volpe, A. *et al.* Ultrasound evaluation of ulnar neuropathy at the elbow: correlation with electrophysiological studies. *Rheumatology (Oxford)* **48**, 1098–1101 (2009).
50. Baumer, P. *et al.* Ulnar neuropathy at the elbow: MR neurography–nerve T2 signal increase and caliber. *Radiology* **260**, 199–206 (2011).
51. Pham, M. *et al.* Anterior interosseous nerve syndrome: fascicular motor lesions of median nerve trunk. *Neurology* **82**, 598–606 (2014).
52. Baumer, P. *et al.* Posterior interosseous neuropathy: supinator syndrome versus fascicular radial neuropathy. *Neurology* **87**, 1884–1891 (2016).
53. Erra, C. *et al.* Secondary posterior interosseous nerve lesions associated with humeral fractures. *Muscle Nerve* **53**, 375–378 (2016).
54. Shahid, K. R. *et al.* Evaluation of intraneural ganglion cysts using three-dimensional fast spin echo-cube. *J. Magn. Reson. Imaging* **32**, 714–718 (2010).
55. Chhabra, A. *et al.* MR neurography findings of soleal sling entrapment. *AJR Am. J. Roentgenol.* **196**, W290–W297 (2011).
56. Du, R., Auguste, K. I., Chin, C. T., Engstrom, J. W. & Weinstein, P. R. Magnetic resonance neurography for the evaluation of peripheral nerve, brachial plexus, and nerve root disorders. *J. Neurosurg.* **112**, 362–371 (2010).
57. Fisher, S., Wadhwa, V., Manthuruthil, C., Cheng, J. & Chhabra, A. Clinical impact of magnetic resonance neurography in patients with brachial plexus neuropathies. *Br. J. Radiol.* **89**, 20160503 (2016).
58. Park, M. S., Kim du, H. & Sung, D. H. Magnetic resonance neurographic findings in classic idiopathic neuralgic amyotrophy in subacute stage: a report of four cases. *Ann. Rehabil. Med.* **38**, 286–291 (2014).
59. Yoshida, T., Sueyoshi, T., Suwazono, S. & Suehara, M. Three-tesla magnetic resonance neurography of the brachial plexus in cervical radiculopathy. *Muscle Nerve* **52**, 392–396 (2015).
60. Seo, T. G., Kim du, H., Kim, I. S. & Son, E. S. Does C5 or C6 radiculopathy affect the signal intensity of the brachial plexus on magnetic resonance neurography? *Ann. Rehabil. Med.* **40**, 362–367 (2016).
61. Aranyi, Z. *et al.* Ultrasonographic identification of nerve pathology in neuralgic amyotrophy: enlargement, constriction, fascicular entwinement, and torsion. *Muscle Nerve* **52**, 503–511 (2015).
62. Lieba-Samal, D., Jengojan, S., Kasprian, G., Wober, C. & Bodner, G. Neuroimaging of classic neuralgic amyotrophy. *Muscle Nerve* **54**, 1079–1085 (2016).
63. Aralasmak, A. *et al.* MRI findings in thoracic outlet syndrome. *Skeletal Radiol.* **41**, 1365–1374 (2012).
64. Demondion, X. *et al.* Thoracic outlet: assessment with MR imaging in asymptomatic and symptomatic populations. *Radiology* **227**, 461–468 (2003).
65. Baumer, P. *et al.* Thoracic outlet syndrome in 3T MR neurography-fibrous bands causing discernible lesions of the lower brachial plexus. *Eur. Radiol.* **24**, 756–761 (2014).
66. Hixson, K. M., Horris, H. B., McLeod, T. C. & Bacon, C. E. The diagnostic accuracy of clinical diagnostic tests for thoracic outlet syndrome. *J. Sport Rehabil.* **24**, 1–14 (2016).
67. Massie, R. *et al.* Diabetic cervical radiculoplexus neuropathy: a distinct syndrome expanding the spectrum of diabetic radiculoplexus neuropathies. *Brain* **135**, 3074–3088 (2012).
68. Cai, Z. *et al.* Radiation-induced brachial plexopathy in patients with nasopharyngeal carcinoma: a retrospective study. *Oncotarget* **7**, 18887–18895 (2016).
69. Qayyum, A., MacVicar, A. D., Padhani, A. R., Revell, P. & Husband, J. E. Symptomatic brachial plexopathy following treatment for breast cancer: utility of MR imaging with surface-coil techniques. *Radiology* **214**, 837–842 (2000).
70. Van den Bergh, P. Y. *et al.* European Federation of Neurological Societies/Peripheral Nerve Society guideline on management of chronic inflammatory demyelinating polyradiculoneuropathy: report of a joint task force of the European Federation of Neurological Societies and the Peripheral Nerve Society — first revision. *Eur. J. Neurol.* **17**, 356–363 (2010).
71. Gasparotti, R. *et al.* Neuroimaging in diagnosis of atypical polyradiculoneuropathies: report of three cases and review of the literature. *J. Neurol.* **262**, 1714–1723 (2015).
72. Shibuya, K. *et al.* Reconstruction magnetic resonance neurography in chronic inflammatory demyelinating polyneuropathy. *Ann. Neurol.* **77**, 333–337 (2015).
73. Kakuda, T. *et al.* Diffusion tensor imaging of peripheral nerve in patients with chronic inflammatory demyelinating polyradiculoneuropathy: a feasibility study. *Neuroradiology* **53**, 955–960 (2011).
74. Markvardsen, L. H., Vaeggemose, M., Ringgaard, S. & Andersen, H. Diffusion tensor imaging can be used to detect lesions in peripheral nerves in patients with chronic inflammatory demyelinating polyneuropathy treated with subcutaneous immunoglobulin. *Neuroradiology* **58**, 745–752 (2016).
75. Joint Task Force of the EFNS and the PNS. European Federation of Neurological Societies/Peripheral Nerve Society guideline on management of multifocal motor neuropathy. Report of a joint task force of the European Federation of Neurological Societies and the Peripheral Nerve Society — first revision. *J. Peripher. Nerv. Syst.* **15**, 295–301 (2010).
76. van Es, H. W. *et al.* Magnetic resonance imaging of the brachial plexus in patients with multifocal motor neuropathy. *Neurology* **48**, 1218–1224 (1997).
77. Ellegala, D. B. *et al.* Characterization of genetically defined types of Charcot–Marie–Tooth neuropathies by using magnetic resonance neurography. *J. Neurosurg.* **102**, 242–245 (2005).
78. Cellerini, M., Salti, S., Desideri, V. & Marconi, G. MR imaging of the cauda equina in hereditary motor sensory neuropathies: correlations with sural nerve biopsy. *AJNR Am. J. Neuroradiol.* **21**, 1793–1798 (2000).
79. Sinclair, C. D. *et al.* MRI shows increased sciatic nerve cross sectional area in inherited and inflammatory neuropathies. *J. Neurol. Neurosurg. Psychiatry* **82**, 1283–1286 (2011).
80. Plante-Bordeneuve, V. & Said, G. Familial amyloid polyneuropathy. *Lancet Neurol.* **10**, 1086–1097 (2011).
81. Adams, D. *et al.* First European consensus for diagnosis, management, and treatment of transthyretin familial amyloid polyneuropathy. *Curr. Opin. Neurol.* **29** (Suppl. 1), S14–S26 (2016).
82. Kollmer, J. *et al. In vivo* detection of nerve injury in familial amyloid polyneuropathy by magnetic resonance neurography. *Brain* **138**, 549–562 (2015).
83. Granata, G. *et al.* Ultrasound evaluation in transthyretin-related amyloid neuropathy. *Muscle Nerve* **50**, 372–376 (2014).
84. Grimm, A. *et al.* Ultrasound pattern sum score, homogeneity score and regional nerve enlargement index for differentiation of demyelinating inflammatory and hereditary neuropathies. *Clin. Neurophysiol.* **127**, 2618–2624 (2016).
85. Sugimoto, T. *et al.* Ultrasonographic nerve enlargement of the median and ulnar nerves and the cervical nerve roots in patients with demyelinating Charcot–Marie–Tooth disease: distinction from patients with chronic inflammatory demyelinating polyneuropathy. *J. Neurol.* **260**, 2580–2587 (2013).
86. Zaidman, C. M., Harms, M. B. & Pestronk, A. Ultrasound of inherited versus acquired demyelinating polyneuropathies. *J. Neurol.* **260**, 3115–3121 (2013).
87. Padua, L. *et al.* Heterogeneity of root and nerve ultrasound pattern in CIDP patients. *Clin. Neurophysiol.* **125**, 160–165 (2014).
88. Kerasnoudis, A., Pitarokoili, K., Haghikia, A., Gold, R. & Yoon, M. S. Nerve ultrasound protocol in differentiating chronic immune-mediated neuropathies. *Muscle Nerve* **54**, 864–871 (2016).
89. Yiu, E. M. *et al.* Peripheral nerve ultrasound in pediatric Charcot–Marie–Tooth disease type 1A. *Neurology* **84**, 569–574 (2015).
90. Grimm, A. *et al.* Ultrasound aspects in therapy-naive CIDP compared to long-term treated CIDP. *J. Neurol.* **263**, 1074–1082 (2016).
91. Zaidman, C. M., Al-Lozi, M. & Pestronk, A. Peripheral nerve size in normals and patients with polyneuropathy: an ultrasound study. *Muscle Nerve* **40**, 960–966 (2009).
92. Goedee, H. S., Brekelmans, G. J. & Visser, L. H. Multifocal enlargement and increased vascularization of peripheral nerves detected by sonography in CIDP: a pilot study. *Clin. Neurophysiol.* **125**, 154–159 (2014).
93. Scheidl, E. *et al.* Ultrasonography of MADSAM neuropathy: focal nerve enlargements at sites of existing and resolved conduction blocks. *Neuromuscul. Disord.* **22**, 627–631 (2012).
94. Beekman, R. *et al.* Ultrasonography shows extensive nerve enlargements in multifocal motor neuropathy. *Neurology* **65**, 305–307 (2005).

95. Kerasnoudis, A., Pitarokoili, K., Behrendt, V., Gold, R. & Yoon, M. S. Multifocal motor neuropathy: correlation of nerve ultrasound, electrophysiological, and clinical findings. *J. Peripher. Nerv. Syst.* **19**, 165–174 (2014).
96. Grimm, A. *et al.* Nerve ultrasound for differentiation between amyotrophic lateral sclerosis and multifocal motor neuropathy. *J. Neurol.* **262**, 870–880 (2015).
97. Loewenbruck, K. F. *et al.* Nerve ultrasound in the differentiation of multifocal motor neuropathy (MMN) and amyotrophic lateral sclerosis with predominant lower motor neuron disease (ALS/LMND). *J. Neurol.* **263**, 35–44 (2016).
98. Lauria, G. & Lombardi, R. Skin biopsy: a new tool for diagnosing peripheral neuropathy. *BMJ* **334**, 1159–1162 (2007).
99. Lauria, G. *et al.* Trigeminal small-fiber sensory neuropathy causes burning mouth syndrome. *Pain* **115**, 332–337 (2005).
100. Gemignani, F. *et al.* Non-length dependent small fiber neuropathy. a prospective case series. *J. Peripher. Nerv. Syst.* **15**, 57–62 (2010).
101. Gorson, K. C. *et al.* Non-length dependent small fibre neuropathy/ganglionopathy. *J. Neurol. Neurosurg. Psychiatry* **79**, 163–169 (2008).
102. Devigili, G. *et al.* The diagnostic criteria for small fibre neuropathy: from symptoms to neuropathology. *Brain* **131**, 1912–1925 (2008).
103. Lauria, G., Merkies, I. S. & Faber, C. G. Small fibre neuropathy. *Curr. Opin. Neurol.* **25**, 542–549 (2012).
104. Gibbons, C. H. & Freeman, R. Treatment-induced neuropathy of diabetes: an acute, iatrogenic complication of diabetes. *Brain* **138**, 43–52 (2015).
105. Cazzato, D. *et al.* Small fiber neuropathy is a common feature of Ehlers-Danlos syndromes. *Neurology* **87**, 155–159 (2016).
106. Faber, C. G. *et al.* Gain of function $Na_v1.7$ mutations in idiopathic small fiber neuropathy. *Ann. Neurol.* **71**, 26–39 (2012).
107. Faber, C. G. *et al.* Gain-of-function $Na_v1.8$ mutations in painful neuropathy. *Proc. Natl Acad. Sci. USA* **109**, 19444–19449 (2012).
108. Huang, J. *et al.* Gain-of-function mutations in sodium channel Nav1.9 in painful neuropathy. *Brain* **137**, 1627–1642 (2014).
109. Han, C. *et al.* Functional profiles of SCN9A variants in dorsal root ganglion neurons and superior cervical ganglion neurons correlate with autonomic symptoms in small fibre neuropathy. *Brain* **135**, 2613–2628 (2012).
110. Martinelli-Boneschi, F. *et al.* COL6A5 variants in familial neuropathic chronic itch. *Brain* http://dx.doi.org/10.1093/brain/aww343 (2017).
111. Tesfaye, S. *et al.* Diabetic neuropathies: update on definitions, diagnostic criteria, estimation of severity, and treatments. *Diabetes Care* **33**, 2285–2293 (2010).
112. Malik, R. *et al.* Small fiber neuropathy: role in the diagnosis of diabetic sensorimotor polyneuropathy. *Diabetes Metab. Res. Rev.* **27**, 678–684 (2011).
113. Dyck, P. J. *et al.* Introduction of automated systems to evaluate touch-pressure, vibration, and thermal cutaneous sensation in man. *Ann. Neurol.* **4**, 502–510 (1978).
114. Fruhstorfer, H., Lindblom, U. & Schmidt, W. C. Method for quantitative estimation of thermal thresholds in patients. *J. Neurol. Neurosurg. Psychiatry* **39**, 1071–1075 (1976).
115. Lauria, G. *et al.* Tubule and neurofilament immunoreactivity in human hairy skin: markers for intraepidermal nerve fibers. *Muscle Nerve* **30**, 310–316 (2004).
116. Lauria, G. *et al.* Expression of capsaicin receptor immunoreactivity in human peripheral nervous system and in painful neuropathies. *J. Peripher. Nerv. Syst.* **11**, 262–271 (2006).
117. Holland, N. R. *et al.* Small-fiber sensory neuropathies: clinical course and neuropathology of idiopathic cases. *Ann. Neurol.* **44**, 47–59 (1998).
118. Nolano, M. *et al.* Quantification of myelinated endings and mechanoreceptors in human digital skin. *Ann. Neurol.* **54**, 197–205 (2003).
119. Nolano, M. *et al.* Quantification of pilomotor nerves. A new tool to evaluate autonomic involvement in diabetes. *Neurology* **75**, 1089–1097 (2010).
120. Gibbons, C. H., Illigens, B. M., Wang, N. & Freeman, R. Quantification of sudomotor innervation: a comparison of three methods. *Muscle Nerve* **42**, 112–119 (2010).
121. McCarthy, B. G. *et al.* Cutaneous innervation in sensory neuropathies: evaluation by skin biopsy. *Neurology* **45**, 1848–1855 (1995).
122. Kennedy, W. R. & Wendelschafer-Crabb, G. The innervation of human epidermis. *J. Neurol. Sci.* **115**, 184–190 (1993).
123. Wang, L., Hilliges, M., Jernberg, T., Wiegleb-Edstrom, D. & Johansson, O. Protein gene product 9.5-immunoreactive nerve fibres and cells in human skin. *Cell Tissue Res.* **261**, 25–33 (1990).
124. McArthur, J. C., Stocks, E. A., Hauer, P., Cornblath, D. R. & Griffin, J. W. Epidermal nerve fiber density: normative reference range and diagnostic efficiency. *Arch. Neurol.* **55**, 1513–1520 (1998).
125. Lauria, G. *et al.* Intraepidermal nerve fiber density at the distal leg: a worldwide normative reference study. *J. Peripher. Nerv. Syst.* **15**, 202–207 (2010).
126. Provitera, V. *et al.* A multi-center, multinational age- and gender-adjusted normative dataset for immunofluorescent intraepidermal nerve fiber density at the distal leg. *Eur. J. Neurol.* **23**, 333–338 (2016).
127. Panoutsopoulou, I. G., Luciano, C. A., Wendelschafer-Crabb, G., Hodges, J. S. & Kennedy, W. R. Epidermal innervation in healthy children and adolescents. *Muscle Nerve* **51**, 378–384 (2015).
128. Lauria, G. *et al.* European Federation of Neurological Societies/Peripheral Nerve Society guideline on the use of skin biopsy in the diagnosis of small fiber neuropathy. *J. Periph. Nerv. Syst.* **15**, 79–92 (2010).
129. Nolano, M. *et al.* Epidermal innervation morphometry by immunofluorescence and bright-field microscopy. *J. Peripher. Nerv. Syst.* **20**, 387–391 (2015).
130. Lauria, G. *et al.* Side and time variability of intraepidermal nerve fiber density. *Neurology* **84**, 2368–2371 (2015).
131. Seger, S. *et al.* A semi-automated method to assess intraepidermal nerve fibre density in human skin biopsies. *Histopathology* **68**, 657–665 (2015).
132. Lauria, G. *et al.* Morphometry of dermal nerve fibers in human skin. *Neurology* **77**, 242–249 (2011).
133. Vlckova-Moravcova, E., Bednarik, J., Dusek, L., Toyka, K. V. & Sommer, C. Diagnostic validity of epidermal nerve fiber densities in painful sensory neuropathies. *Muscle Nerve* **37**, 50–60 (2008).
134. Provitera, V. *et al.* Myelinated nerve endings in human skin. *Muscle Nerve* **35**, 767–775 (2007).
135. Manganelli, F. *et al.* Charcot–Marie–Tooth disease: new insights from skin biopsy. *Neurology* **85**, 1202–1208 (2015).
136. Nolano, M. *et al.* Small nerve fiber involvement in CMT1A. *Neurology* **84**, 407–414 (2015).
137. Gibbons, C. H., Illigens, B. M., Wang, N. & Freeman, R. Quantification of sweat gland innervation: a clinical-pathologic correlation. *Neurology* **72**, 1479–1486 (2009).
138. Chao, C. C. *et al.* Sudomotor innervation in transthyretin amyloid neuropathy: pathology and functional correlates. *Ann. Neurol.* **78**, 272–283 (2015).
139. Liu, Y. *et al.* Factors influencing sweat gland innervation in diabetes. *Neurology* **84**, 1652–1659 (2015).
140. Sommer, C., Lindenlaub, T., Zillikens, D., Toyka, K. V. & Naumann, M. Selective loss of cholinergic sudomotor fibers causes anhidrosis in Ross syndrome. *Ann. Neurol.* **52**, 247–250 (2002).
141. Nolano, M. *et al.* Ross syndrome: a rare or a misknown disorder of thermoregulation? A skin innervation study on 12 subjects. *Brain* **129**, 2119–2131 (2006).
142. Donadio, V. *et al.* Anhidrosis in multiple system atrophy: a preganglionic sudomotor dysfunction? *Mov. Disord.* **23**, 885–888 (2008).
143. Provitera, V. *et al.* Postganglionic sudomotor denervation in patients with multiple system atrophy. *Neurology* **82**, 2223–2229 (2014).
144. Nolano, M. *et al.* Sensory deficit in Parkinson's disease: evidence of a cutaneous denervation. *Brain* **131**, 1903–1911 (2008).
145. Doppler, K. *et al.* Cutaneous neuropathy in Parkinson's disease: a window into brain pathology. *Acta Neuropathol.* **128**, 99–109 (2014).
146. Weis, J. *et al.* Small-fiber neuropathy in patients with ALS. *Neurology* **76**, 2024–2029 (2011).
147. Nolano, M. *et al.* Nonmotor involvement in amyotrophic lateral sclerosis: new insight from nerve and vessel analysis in skin biopsy. *Neuropathol. Appl. Neurobiol.* http://dx.doi.org/10.1111/nan.12332 (2016).
148. Dalla Bella, E. *et al.* Amyotrophic lateral sclerosis causes small fiber pathology. *Eur. J. Neurol.* **23**, 416–420 (2016).
149. Truini, A. *et al.* Small-fibre neuropathy related to bulbar and spinal-onset in patients with ALS. *J. Neurol.* **262**, 1014–1018 (2015).
150. Sassone, J. *et al.* ALS mouse model SOD1G93A displays early pathology of sensory small fibers associated to accumulation of a neurotoxic splice variant of peripherin. *Hum. Mol. Genet.* **25**, 1588–1599 (2016).
151. Al-Zuhairy, A., Schroder, H. D., Plesner, T., Abildgaard, N. & Sindrup, S. H. Immunostaining of skin biopsy adds no diagnostic value in MGUS-associated peripheral neuropathy. *J. Neurol. Sci.* **349**, 60–64 (2015).
152. Lombardi, R. *et al.* IgM deposits on skin nerves in anti-myelin-associated glycoprotein neuropathy. *Ann. Neurol.* **57**, 180–187 (2005).
153. Stalder, A. K. *et al.* Immunoglobulin M deposition in cutaneous nerves of anti-myelin-associated glycoprotein polyneuropathy patients correlates with axonal degeneration. *J. Neuropathol. Exp. Neurol.* **68**, 148–158 (2009).
154. Ruts, L. *et al.* Unmyelinated and myelinated skin nerve damage in Guillain–Barre syndrome: correlation with pain and recovery. *Pain* **153**, 399–409 (2012).
155. Oliveira-Soto, L. & Efron, N. Morphology of corneal nerves using confocal microscopy. *Cornea* **20**, 374–384 (2001).
156. Muller, L. J., Marfurt, C. F., Kruse, F. & Tervo, T. M. Corneal nerves: structure, contents and function. *Exp. Eye Res.* **76**, 521–542 (2003).
157. Tavakoli, M., Petropoulos, I. N. & Malik, R. A. Corneal confocal microscopy to assess diabetic neuropathy: an eye on the foot. *J. Diabetes Sci. Technol.* **7**, 1179–1189 (2013).
158. Petroll, W. M., Weaver, M., Vaidya, S., McCulley, J. P. & Cavanagh, H. D. Quantitative 3-dimensional corneal imaging *in vivo* using a modified HRT-RCM confocal microscope. *Cornea* **32**, e36–e43 (2013).
159. Petropoulos, I. N. *et al.* Rapid automated diagnosis of diabetic peripheral neuropathy with *in vivo* corneal confocal microscopy. *Invest. Ophthalmol. Vis. Sci.* **55**, 2071–2078 (2014).
160. Dehghani, C. *et al.* Fully automated, semiautomated, and manual morphometric analysis of corneal subbasal nerve plexus in individuals with and without diabetes. *Cornea* **33**, 696–702 (2014).
161. Dabbah, M. A., Graham, J., Petropoulos, I. N., Tavakoli, M. & Malik, R. A. Automatic analysis of diabetic peripheral neuropathy using multi-scale quantitative morphology of nerve fibres in corneal confocal microscopy imaging. *Med. Image Anal.* **15**, 738–747 (2011).
162. Tavakoli, M. *et al.* Normative values for corneal nerve morphology assessed using corneal confocal microscopy: a multinational normative data set. *Diabetes Care* **38**, 838–843 (2015).
163. Hossain, P., Sachdev, A. & Malik, R. A. Early detection of diabetic peripheral neuropathy with corneal confocal microscopy. *Lancet* **366**, 1340–1343 (2005).
164. Quattrini, C. *et al.* Surrogate markers of small fiber damage in human diabetic neuropathy. *Diabetes* **56**, 2148–2154 (2007).
165. Wu, T. *et al.* Variables associated with corneal confocal microscopy parameters in healthy volunteers: implications for diabetic neuropathy screening. *Diabet. Med.* **29**, e297–e303 (2012).
166. Ziegler, D. *et al.* Early detection of nerve fiber loss by corneal confocal microscopy and skin biopsy in recently diagnosed type 2 diabetes. *Diabetes* **63**, 2454–2463 (2014).
167. Tavakoli, M. *et al.* Corneal confocal microscopy detects small-fiber neuropathy in Charcot–Marie–Tooth disease type 1A patients. *Muscle Nerve* **46**, 698–704 (2012).
168. Mimura, T. *et al. In vivo* confocal microscopy of hereditary sensory and autonomic neuropathy. *Curr. Eye Res.* **33**, 940–945 (2008).
169. Tavakoli, M. *et al.* Corneal confocal microscopy: a novel noninvasive means to diagnose neuropathy in patients with Fabry disease. *Muscle Nerve* **40**, 976–984 (2009).
170. Lalive, P. H., Truffert, A., Magistris, M. R., Landis, T. & Dosso, A. Peripheral autoimmune neuropathy assessed using corneal *in vivo* confocal microscopy. *Arch. Neurol.* **66**, 403–405 (2009).
171. Ferrari, G., Gemignani, F. & Macaluso, C. Chemotherapy-associated peripheral sensory neuropathy assessed using *in vivo* corneal confocal microscopy. *Arch. Neurol.* **67**, 364–365 (2010).
172. Chen, X. *et al.* Small nerve fiber quantification in the diagnosis of diabetic sensorimotor polyneuropathy: comparing corneal confocal microscopy with intraepidermal nerve fiber density. *Diabetes Care* **38**, 1138–1144 (2015).

173. Tavakoli, M. *et al.* Corneal confocal microscopy detects improvement in corneal nerve morphology with an improvement in risk factors for diabetic neuropathy. *Diabet. Med.* **28**, 1261–1267 (2011).
174. Tavakoli, M. *et al.* Corneal confocal microscopy detects early nerve regeneration in diabetic neuropathy after simultaneous pancreas and kidney transplantation. *Diabetes* **62**, 254–260 (2013).
175. Mehra, S. *et al.* Corneal confocal microscopy detects early nerve regeneration after pancreas transplantation in patients with type 1 diabetes. *Diabetes Care* **30**, 2608–2612 (2007).
176. Le Pera, D., Valeriani, M., Niddam, D., Chen, A. C. & Arendt-Nielsen, L. Contact heat evoked potentials to painful and non-painful stimuli: effect of attention towards stimulus properties. *Brain Topogr.* **15**, 115–123 (2002).
177. Katsarava, Z. *et al.* A novel method of eliciting pain-related potentials by transcutaneous electrical stimulation. *Headache* **46**, 1511–1517 (2006).
178. Inui, K. & Kakigi, R. Pain perception in humans: use of intraepidermal electrical stimulation. *J. Neurol. Neurosurg. Psychiatry* **83**, 551–556 (2012).
179. Kodaira, M., Inui, K. & Kakigi, R. Evaluation of nociceptive Aδ⁻ and C-fiber dysfunction with lidocaine using intraepidermal electrical stimulation. *Clin. Neurophysiol.* **125**, 1870–1877 (2014).
180. Valeriani, M., Pazzaglia, C., Cruccu, G. & Truini, A. Clinical usefulness of laser evoked potentials. *Neurophysiol. Clin.* **42**, 345–353 (2012).
181. Cruccu, G. *et al.* Recommendations for the clinical use of somatosensory-evoked potentials. *Clin. Neurophysiol.* **119**, 1705–1719 (2008).
182. Garcia-Larrea, L., Peyron, R., Laurent, B. & Mauguiere, F. Association and dissociation between laser-evoked potentials and pain perception. *Neuroreport* **8**, 3785–3789 (1997).
183. Bragard, D., Chen, A. C. & Plaghki, L. Direct isolation of ultra-late (C-fibre) evoked brain potentials by CO2 laser stimulation of tiny cutaneous surface areas in man. *Neurosci. Lett.* **209**, 81–84 (1996).
184. Cruccu, G. *et al.* Unmyelinated trigeminal pathways as assessed by laser stimuli in humans. *Brain* **126**, 2246–2256 (2003).
185. Plaghki, L. & Mouraux, A. How do we selectively activate skin nociceptors with a high power infrared laser? Physiology and biophysics of laser stimulation. *Neurophysiol. Clin.* **33**, 269–277 (2003).
186. Kakigi, R., Inui, K. & Tamura, Y. Electrophysiological studies on human pain perception. *Clin. Neurophysiol.* **116**, 743–763 (2005).
187. Granovsky, Y., Matre, D., Sokolik, A., Lorenz, J. & Casey, K. L. Thermoreceptive innervation of human glabrous and hairy skin: a contact heat evoked potential analysis. *Pain* **115**, 238–247 (2005).
188. Casanova-Molla, J., Grau-Junyent, J. M., Morales, M. & Valls-Sole, J. On the relationship between nociceptive evoked potentials and intraepidermal nerve fiber density in painful sensory polyneuropathies. *Pain* **152**, 410–418 (2011).
189. Arendt-Nielsen, L. & Chen, A. C. Lasers and other thermal stimulators for activation of skin nociceptors in humans. *Neurophysiol. Clin.* **33**, 259–268 (2003).
190. Atherton, D. D. *et al.* Use of the novel contact heat evoked potential stimulator (CHEPS) for the assessment of small fibre neuropathy: correlations with skin flare responses and intra-epidermal nerve fibre counts. *BMC Neurol.* **7**, 21 (2007).
191. Chen, A. C., Niddam, D. M. & Arendt-Nielsen, L. Contact heat evoked potentials as a valid means to study nociceptive pathways in human subjects. *Neurosci. Lett.* **316**, 79–82 (2001).
192. Lagerburg, V. *et al.* Contact heat evoked potentials: normal values and use in small fiber neuropathy. *Muscle Nerve* **51**, 743–749 (2014).
193. Obermann, M. *et al.* Correlation of epidermal nerve fiber density with pain-related evoked potentials in HIV neuropathy. *Pain* **138**, 79–86 (2008).
194. Mueller, D. *et al.* Electrically evoked nociceptive potentials for early detection of diabetic small-fiber neuropathy. *Eur. J. Neurol.* **17**, 834–841 (2010).
195. Oh, K. J. *et al.* Pain-related evoked potential in healthy adults. *Ann. Rehabil. Med.* **39**, 108–115 (2015).
196. Serra, J. The role of neurophysiology. *J. Peripher. Nerv. Syst.* **19** (Suppl. 2), S22–S24 (2014).
197. Serra, J., Campero, M., Bostock, H. & Ochoa, J. Two types of C nociceptors in human skin and their behavior in areas of capsaicin-induced secondary hyperalgesia. *J. Neurophysiol.* **91**, 2770–2781 (2004).
198. Serra, J. *et al.* Double and triple spikes in C-nociceptors in neuropathic pain states: an additional peripheral mechanism of hyperalgesia. *Pain* **152**, 343–353 (2011).
199. Serra, J. *et al.* Microneurographic identification of spontaneous activity in C-nociceptors in neuropathic pain states in humans and rats. *Pain* **153**, 42–55 (2012).
200. Serra, J. *et al.* C-Nociceptors sensitized to cold in a patient with small-fiber neuropathy and cold allodynia. *Pain* **147**, 46–53 (2009).
201. Serra, J., Campero, M., Ochoa, J. & Bostock, H. Activity-dependent slowing of conduction differentiates functional subtypes of C fibres innervating human skin. *J. Physiol.* **515**, 799–811 (1999).
202. Serra, J. *et al.* Hyperexcitable C nociceptors in fibromyalgia. *Ann. Neurol.* **75**, 196–208 (2014).
203. Kleggetveit, I. P. *et al.* High spontaneous activity of C-nociceptors in painful polyneuropathy. *Pain* **153**, 2040–2047 (2012).
204. Hoitsma, E. *et al.* Abnormal warm and cold sensation thresholds suggestive of small-fiber neuropathy in sarcoidosis. *Clin. Neurophysiol.* **114**, 2326–2333 (2003).
205. Hoeijmakers, J. G., Faber, C. G., Lauria, G., Merkies, I. S. & Waxman, S. G. Small-fibre neuropathies-advances in diagnosis, pathophysiology and management. *Nat. Rev. Neurol.* **8**, 369–379 (2012).
206. Hansson, P., Backonja, M. & Bouhassira, D. Usefulness and limitations of quantitative sensory testing: clinical and research application in neuropathic pain states. *Pain* **129**, 256–259 (2007).
207. Shy, M. E. *et al.* Quantitative sensory testing: report of the Therapeutics and Technology Assessment Subcommittee of the American Academy of Neurology. *Neurology* **60**, 898–904 (2003).
208. Yarnitsky, D., Sprecher, E., Tamir, A., Zaslansky, R. & Hemli, J. A. Variance of sensory threshold measurements: discrimination of feigners from trustworthy performers. *J. Neurol. Sci.* **125**, 186–189 (1994).
209. Verdugo, R. J. & Ochoa, J. L. Use and misuse of conventional electrodiagnosis, quantitative sensory testing, thermography, and nerve blocks in the evaluation of painful neuropathic syndromes. *Muscle Nerve* **16**, 1056–1062 (1993).
210. Maier, C. *et al.* Quantitative sensory testing in the German Research Network on Neuropathic Pain (DFNS): somatosensory abnormalities in 1236 patients with different neuropathic pain syndromes. *Pain* **150**, 439–450 (2010).
211. Chong, P. S. & Cros, D. P. Technology literature review: quantitative sensory testing. *Muscle Nerve* **29**, 734–747 (2004).
212. Bakkers, M. *et al.* Temperature threshold testing: a systematic review. *J. Peripher. Nerv. Syst.* **18**, 7–18 (2013).
213. Backonja, M. M. *et al.* Value of quantitative sensory testing in neurological and pain disorders: NeuPSIG consensus. *Pain* **154**, 1807–1819 (2013).
214. Pan, C. *et al.* Cutaneous innervation in Guillain-Barrē syndrome: pathology and clinical correlations. *Brain* **126**, 386–397 (2003).
215. Pittenger, G. L. *et al.* Intraepidermal nerve fibers are indicators of small-fiber neuropathy in both diabetic and nondiabetic patients. *Diabetes Care* **27**, 1974–1979 (2004).
216. Shun, C. T. *et al.* Skin denervation in type 2 diabetes: correlations with diabetic duration and functional impairments. *Brain* **127**, 1593–1605 (2004).
217. Sorensen, L., Molyneaux, L. & Yue, D. K. The level of small nerve fiber dysfunction does not predict pain in diabetic neuropathy: a study using quantitative sensory testing. *Clin. J. Pain* **22**, 261–265 (2006).
218. Periquet, M. I. *et al.* Painful sensory neuropathy: prospective evaluation using skin biopsy. *Neurology* **53**, 1641–1647 (1999).
219. Holland, N. *et al.* Intraepidermal nerve fibre density in patients with painful sensory neuropathy. *Neurology* **48**, 708–711 (1997).
220. Facer, P. *et al.* Correlation of quantitative tests of nerve and target organ dysfunction with skin immunohistology in leprosy. *Brain* **121**, 2239–2247 (1998).

Author contributions
R.G., L.P. and G.L. wrote the article. All authors researched data for the article, made substantial contributions to discussion of the content and reviewed and/or edited the manuscript before submission.

Competing interests statement
The authors declare no competing interests.